École Polytechnique Fédérale de Lausanne

Laboratory of Ecohydrology ECHO

Master thesis

Investigating temporary streamflow formation in a headwater catchment of the Swiss Mentue river

---

Student:

Nathan Bonnet

Supervisors:

Jana von Freyberg

Izabela Bujak

July 29, 2022

Abstract

Temporary stream networks undergo spatio-temporal variations as some portions of the network alternatively cease and restart to flow. The drainage density, defined as the actively flowing stream length divided by the catchment area constitutes a measure of the stream network variations. However, the volume of data required to accurately calculate drainage density with a high temporal resolution complicates its study. Conversely, measuring the discharge at the outlet of the stream network only requires one point of measure and can be automated. Previous studies suggested that power-law relationship between drainage density and catchment discharge exist. However, they were based on sporadic mapping surveys. Thus, little is known about the short-term variations in drainage density. Does the relationship holds on a timescale of a month or during a rainfall event ? Therefore, this Master thesis investigates the short-term temporal dynamic of the drainage density in the Swiss headwater catchment Bois-Vuacoz (25 ha), in regards with precipitation event characteristics and catchment wetness. It studies empirical relationships between the drainage density and both the discharge at the catchment outlet and the groundwater table level. Such relationships could simplify the high temporal resolution gathering of information on expansion and contraction of the temporary stream network.

To gather data on the presence and absence of streamflow, I installed pressure transducers, electrical resistivity (ER), and flow sensors in 17 locations along the stream network. Using data from pre-existing mapping surveys made at various catchment wetness, I allocated each stream reach of the network to the sensor location with the closest variations in hydrological state. Calculating the length of each reach, I computed the drainage density with a time resolution of 10 minutes. I measured as well the discharge at the outlet of the catchment, the groundwater level close to the main stream and used precipitation from a nearby pluviometric station.

The high temporal resolution of the data revealed that a power-law function did not accurately represent the relationship between the drainage density and the discharge. The model I used reproduced the behavior of drainage density at low and high discharges for which the drainage density remains constant at its minimum level, resp. maximum level. In between these constant segments of drainage density, I modelled the variations of drainage density in regards with discharge by using a power-law relationship. However, the existence of an hysteresis loop between these variables at the timescale of a rainfall event created dispersion of the data around the power-law which remains unexplained by the model. I used a similar model for groundwater level with more contrasting results. The possibility to focus on individual rainfall event revealed a positive correlation between drainage density variation and antecedent wetness as well as precipitation amount.

Contents

List of Figures

List of Tables

1 Introduction

Headwaters designate the uppermost part of watersheds. They are composed of a variety of streams, characterized by a wide spectrum of flow permanency. Temporary streams are among them.

Temporary stream is a term encompassing three types of streams : intermittent, ephemeral and episodic. (Nadeau and Rains 2007). Intermittent streams flow when the groundwater table is sufficiently high to reach the bottom of the stream channel. Ephemeral and episodic streams are situated above the groundwater level at all time, their flow is only fed through superficial flow paths generated by precipitation events or during snow melts (Peirce and Lindsay 2015). Temporary streams react to increase in moisture conditions by expanding in their geomorphological channel and to drier periods by contracting (Godsey and Kirchner 2014). High spatial and temporal variability of these streams create a range of environmental conditions. Temporary streams are ecologically valuable (Acuña et al. 2014), they host a high biodiversity (Meyer et al. 2007) and in particular they provide an habitat to a range of endemic species (Stubbington et al. 2017). They also serve as connectivity corridors (Rinaldo, Gatto, and Rodriguez-Iturbe 2018) and are unique zones of nutrient and carbon exchanges (Schiller et al. 2017).

Variability of temporary streams, often coupled with their remote location and difficulty of access, causes them to be a difficult subject for scientific studies. After mostly inconclusive research in the 70s to determine the empirical laws governing their expansion and contraction, the interest for temporary streams faded for several decades (Godsey and Kirchner 2014). Nevertheless, the scientific community started to regain interest in the study of temporary streams, acknowledging their importance (Creed et al. 2017), and working toward a better understanding of their hydrological behavior (Meerveld et al. 2019), as a key part of the river network.

Expansion and contraction of temporary streams has been linked to physical characteristics of the catchment where they occur (Day 1978). Catchment steepness influences water retention and velocity. Infiltration capacity coupled with soil depth governs subsurface flow and storage capacity. Groundwater depth is directly linked to the preferential patterns of expansion and contraction of particular catchments. (Day 1978).

A complete understanding of temporary stream expansion and contraction requires to identify the processes governing stream network expansion and contraction. Three types of expansion have been described (summarized by Goulsbra, Evans, and J. Lindsay 2014). The "bottom-up" expansion designates the pattern in which, as the catchment becomes wetter, the groundwater table rises progressively, initiating an up-slope motion of the surface flow starting from the bottom of the catchment and extending progressively upward, leading more and more geomorphological channels to be supplied by the groundwater table.

The "top-down" expansion describes a motion where, as the catchment becomes wetter, the upward part reaches a saturation state first, for instance due to a soil with poor water storage capacity. This results in a surface flow that "spills" progressively downward. Finally, the disjointed pattern of expansion is a combination of the previous pattern when they happen simultaneously in different locations and altitude of the catchment.

This Master thesis is part of the TempAqua research project that explores the hydrology of temporary streams in different Swiss catchments. I conducted my Master thesis project in the Bois-Vuacoz headwatershed to address the following research questions :

- How much does the flowing stream network in the Bois-Vuacoz catchment change across space and time during and between rainfall events?
- Can these changes be predicted based on catchment discharge or groundwater table variations?
- How are stream network expansion and contraction linked to antecedent wetness conditions and rainfall properties?

In order to address these questions, I defined the following research objectives :

- Estimate the drainage density with a 10 minutes temporal resolution.
- Identify the expansion and contraction phases of the stream network during the monitoring period.
- Isolate and characterise each rainfall event during the monitoring period.
- Characterize the relationship between drainage density and rainfall events and their properties such as precipitation amount, duration and average intensity.
- Model the relationships between drainage density and discharge as well as groundwater level, with the aim to derive the drainage density from these variables that are simpler to measure.

2 Material and methods

2.1 Study site

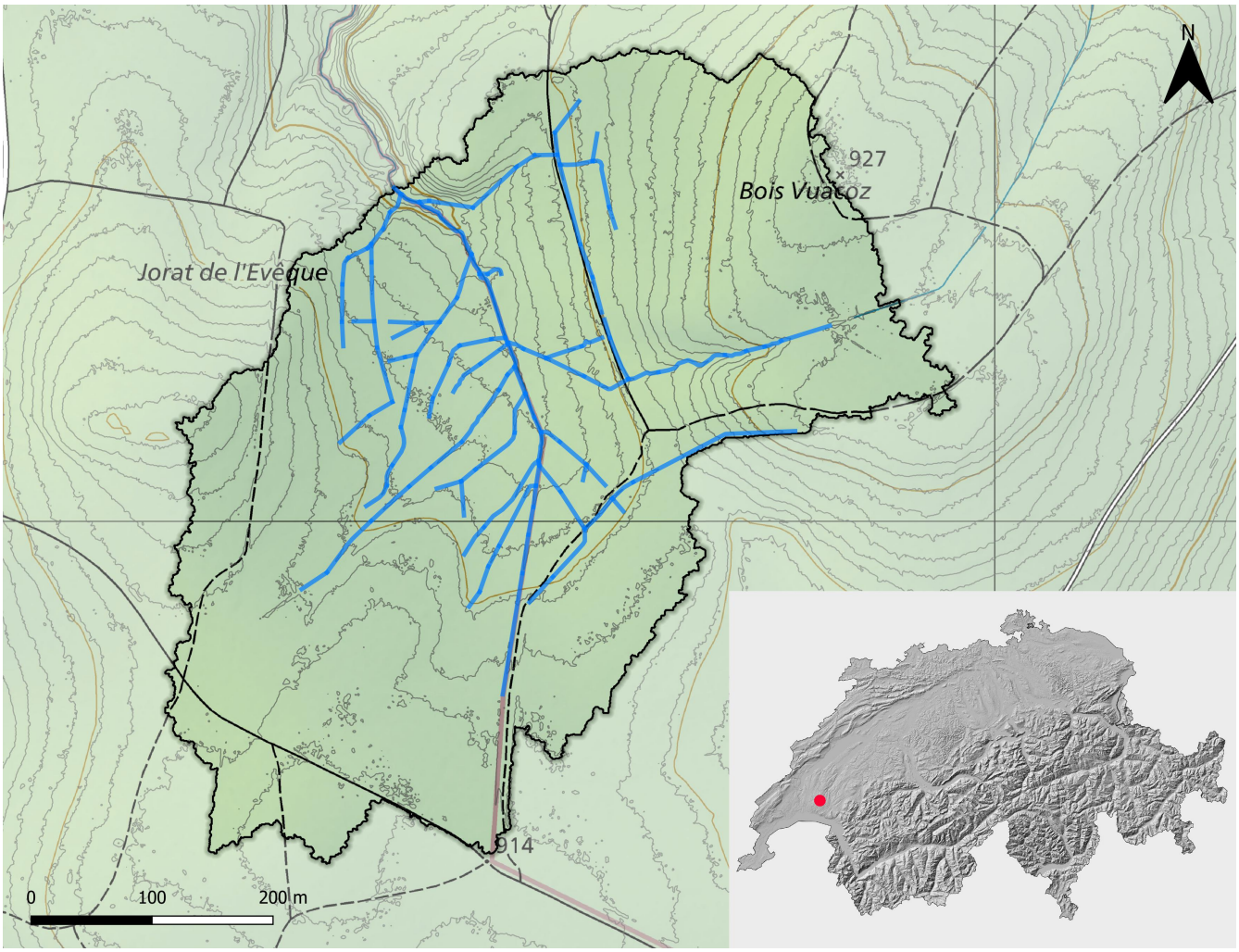

Figure 1: Bois-Vuacoz catchment boundaries and the stream network. The stream network mapping is the result of field work realised by R.Angeles as part of a semester project in the ECHO lab (Angeles 2022). Background map : National map, format 1:10000, by Swisstopo (available on map.geo.admin.ch).

Bois-Vuacoz catchment (abbreviated to BV catchment), Fig.1, is a small experimental headwater catchment situated on the western Swiss Plateau, in the canton of Vaud. It constitutes the uppermost part of of the Mentue watershed, with the Mentue river flowing north into Neuchatel Lake.

BV catchment covers an area of 25.03 ha. Its elevation ranges from 889 to 927 m a.s.l. (Angeles 2022). Bois-Vuacoz is characterised shallow slope with a median steepness of 1.57° and maxmium of 6.61° (Joerin 2000). The Jorat forest covers the entirety of the catchment. The dominant species of tree is spruce, accompanied by native species such as fir and beech. These two species are typical in mixed forests found at montane elevations. Annual precipitation normals on the period 1991-2020 for at the nearby

Meteoswiss meteo station of Villars-Tiercelin amount to 1362 mm (*Normal values per measured parameter - MeteoSwiss* 2022) and precipitation ($\geq$1[mm]) occur on average 130.4 days per year. The Swiss Plateau is characterised by a humid and temperate climate with a continental tendency at Bois-Vuacoz elevation (Joerin 2000). Annual air temperature averages 7°C in the Haute-Mentue catchment (Joerin 2000).

According to the Vaud mapping desk (*Guichet cartographique du canton de Vaud* 2022), Bois-Vuacoz soils are silty to sandy. The soil depth is fairly superficial near the main channel catchment (30-50 cm) and moderately deep (50-70 cm) or even deep(70-100 cm) at higher elevations. Underneath the soil, the bedrock covering the catchment area is almost homogeneously a marly and sandy moraine.

2.2 Instrumentation

I installed two types of sensors to gather information on the evolution of the hydrological conditions and the stream network during the monitoring period. In addition, I used the data collected by pre-existing devices.

2.2.1 Multi-sensor device

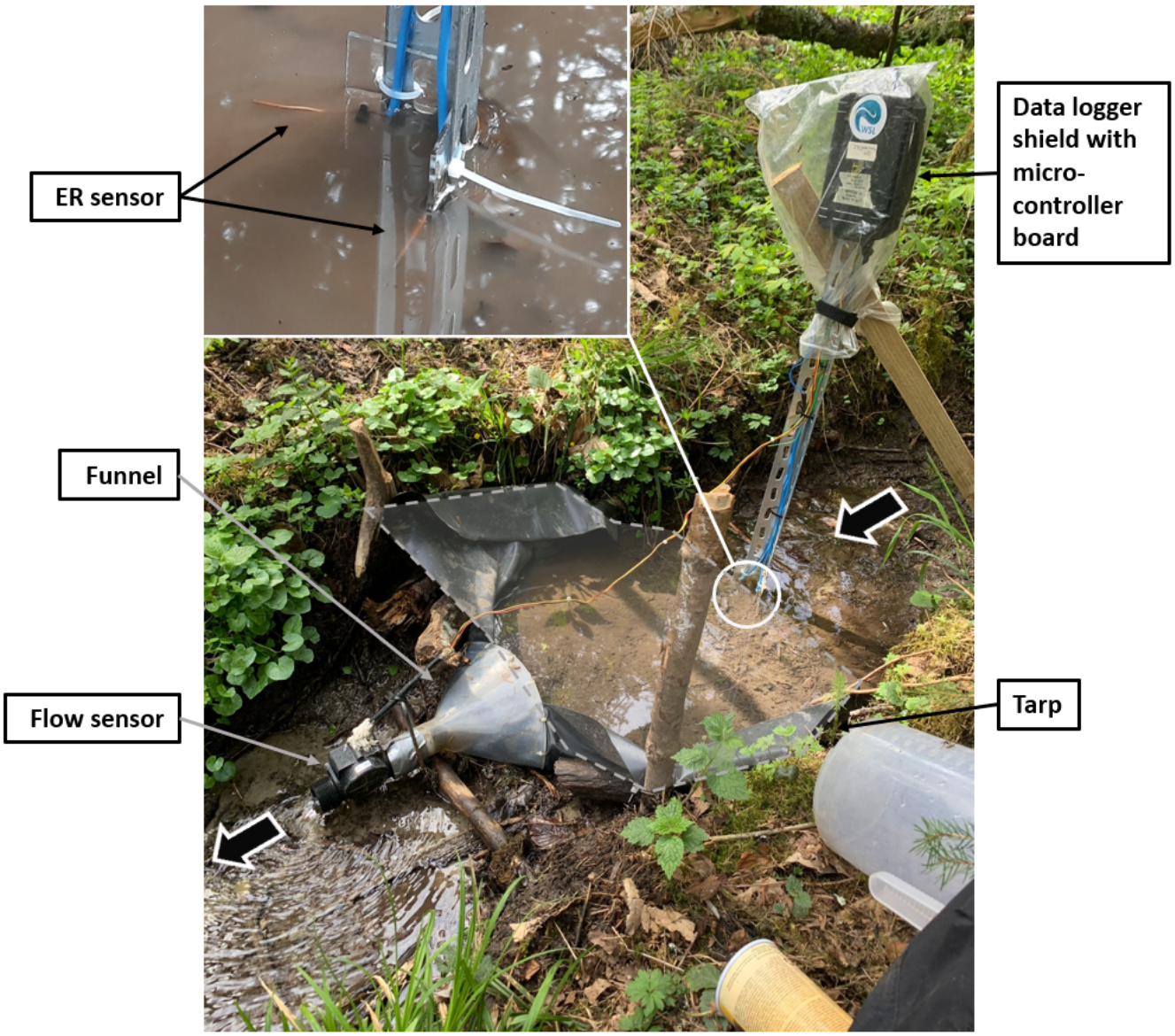

Figure 2: Detailed installation of a multi-sensor device. Picture from location B8.

The multi-sensor device, see Fig. 2, is in fact the assembly of two types of sensors. Assendelft and van Meerveld developed this monitoring system for temporary streams (Assendelft and van Meerveld 2019). Both sensors perform their measurement simultaneously every 5 minutes. The first type measures the electrical resistance (ER) between two copper electrodes (wire diameter of 1.8 mm) separated by a few centimeters. I suspended the electrodes ca.1 cm above the channel bed. In presence of water, the electrical

resistance lowers significantly compared to dry conditions. Thus, this sensor allows to detect if water is present int the stream or not.

Ca.40 cm downstream of the ER sensor, I placed a flow sensor (YIFA Plastic Products Co., ltd, Yuè, Foshan, China). It measures the discharge (volume of water per unit of time) in the stream channel. According to the manufacturer, the range of flow rates measured is 1-120 L/min with an error of $\pm 5\%$ on the measurement. The flow sensor is designed in such a way that a measurement value of 13 L/min marks the threshold between flow and no flow. Measurements above this threshold represent real discharge values while measurements of 13 L/min and below signify the absence of flow. To ensure the capture of most of the flowing water in the stream, I installed an impermeable tarp to seal the bottom and the banks of the channel, forcing the water to circulate directly into a funnel whose exits is tightly attached to the inlet of the flow sensor. The sensor uses an impeller equipped with a magnet. As the water spins the impeller, a fixed Hall-effect measures the frequency of rotation by switching state in response to the polarity alternation. The discharge is directly derived from the switching frequency.

2.2.2 Pressure transducer sensor

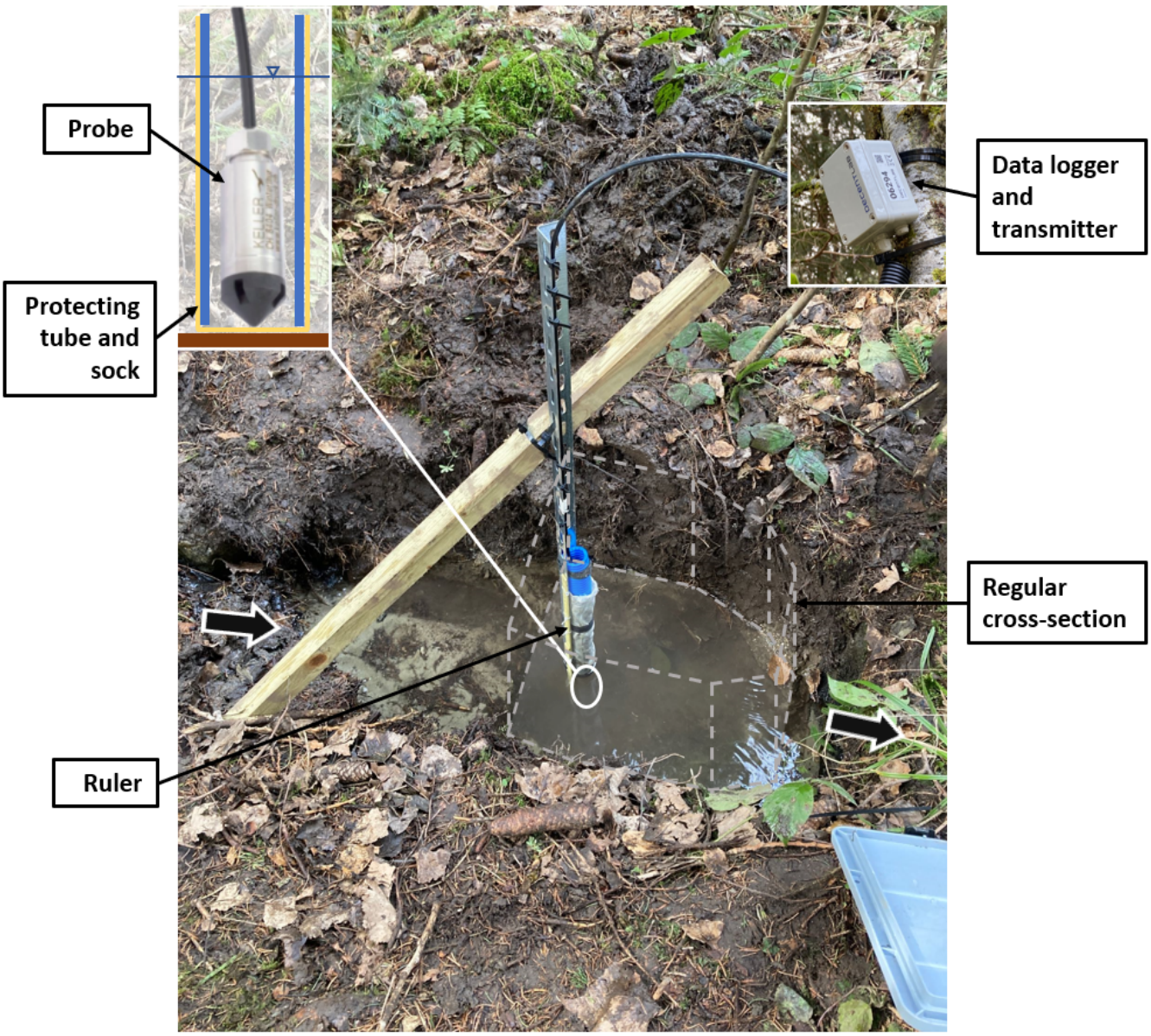

Figure 3: Detailed installation of a water-level sensor. Picture from location B7.

The model used is a hydrostatic level transmitter 26Y series (KELLER Druckmesstechnik AG, Wintertur, Switzerland). The sensor has a measurement interval of 10 minutes. The pressure range is 0-1 bar with an accuracy of ±0.25% of the full-scale range. The level probe uses a piezoresistive technology to measure the hydrostatic pressure of the water column in which it is immersed. The pressure transducer is equipped with a logger DL-PR26 from Decentlab (Decentlab GmbH, Dübendorf, Switzerland) which powers the sensor and uses a radio technology to transmit the data.

I used the pressure transducer sensor for two purposes. First, I used the sensor to derive the water-level in streams. I held the probe vertically in the stream and fixed it to ensure a constant distance to the bottom of the channel. I placed a protective tube around the probe to prevent any coarse material

to collide and interfere with the probe operation. I installed a protective fabric around the tube to stop sediment accumulation between the probe an the inner walls of the tube.

Secondly, I measured the level of the groundwater table at ca.10 m of the upper-section of the main stream channel, see BGW1 in Fig. 6. I installed a screened pipe up to 2 meters deep into the ground and placed the sensor at the bottom.

For both usages, I converted pressure measurements in bar to meter of water column.

2.2.3 Pre-existing devices

In 1992, the former EPFL laboratory HYDRAM has installed an H-flume weir at Bois-Vuacoz outlet (*Haute-Mentue catchment* 2005). A differential pressure transducer HyMADD hydrological measuring station (MADD Technologies Sàrl, Avenue des Sports 42, 1400 Yverdon-les-Bains, Suisse) is mounted in a recess of the flume. The pressure measurement is converted into water-level using a discharge rating curve (Fig. A.1). The level measurement range of the device is 0.03 to 3.05 m and the accuracy varies between ± 0.3 and ± 0.6 mm. From 1997 to 2016, ECHO lab researchers have performed a series of simultaneous water-level and discharge measurements, for the latter using either NaCl or volumetric measurement technique from which I constructed the discharge rating curve (Fig. A.1).

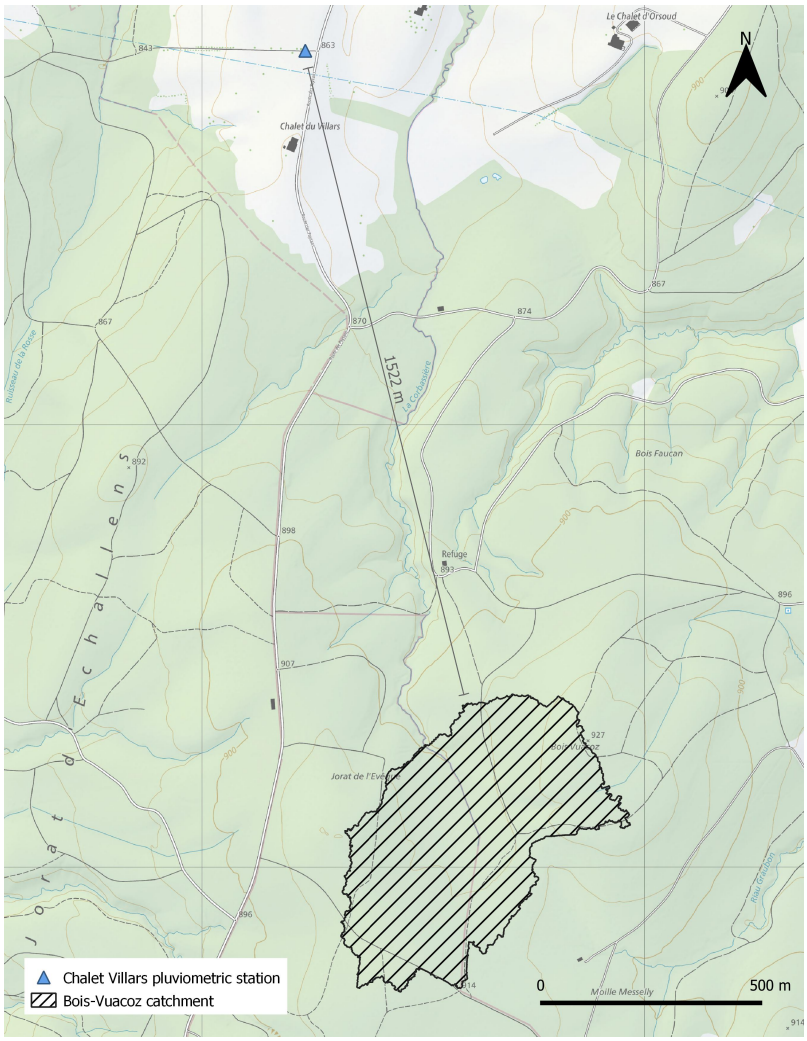

Figure 4: Locations of Chalet Villars pluviometric station and Bois-Vuacoz catchment. Background map : National map, format 1:10000, by Swisstopo (available on map.geo.admin.ch).

The pluviometric station of Chalet Villars, 863 m a.s.l., is in function since 1987. The pluviometer is a tipping-bucket rain gauge with a resolution of 0.1 mm and a collecting surface of 200 cm^2 (Joerin, 2000). 1.5 km separate the station and the north-eastern boundary of Bois-Vuacoz, see figure 4.

2.3 Maintenance and data collection

Data recorded by ER and flow sensors are stored in a SD card. I performed a bi-weekly data collection, immediately followed by sensors reboot and test. On these occasions, I cleaned the tarp from any sediment accumulation and cleared the entrance of the funnel from debris brought by flow.

The data logger connected to the water-level sensor directly emits its data via the Swisscom network to the server, without storing it locally. However, the Bois-Vuacoz catchment is situated in a remote area and sensors are surrounded by tall trees. Some connection issues have been experienced throughout the

monitoring period, leading to a loss of a data. Data gaps ranged from a few dozen minutes up to two weeks. I filled some of theses data gaps by using other data. These points will be further discussed in section 2.8.

In order to obtain discharge rating curves, I installed sensors in locations with well-defined cross sections and stable stream beds. When this was not possible, I installed V-notch weirs into the stream. A long impermeable tarp guides the flow toward the inlet of the V-notch weir box. The sensor is mounted on the inside of the box and protected by a plastic tube (Fig. 5). For both configurations, I regularly cleaned the sediments accumulating around the probe. Any sediment accumulation can alter the pressure and shift the measurements made by the sensor.

Figure 5: Alternative water-level sensor installation inside a V-notch weir box. In black, the tarp is connected to the inlet of the weir box and collect the flow coming from upstream.

The analysis performed during this master thesis comes from the data gathered during the monitoring period beginning on the 22th of April and finishing on the 23rd of May, both days included. The monitoring period lasts exactly 32 days.

2.4 Monitoring locations

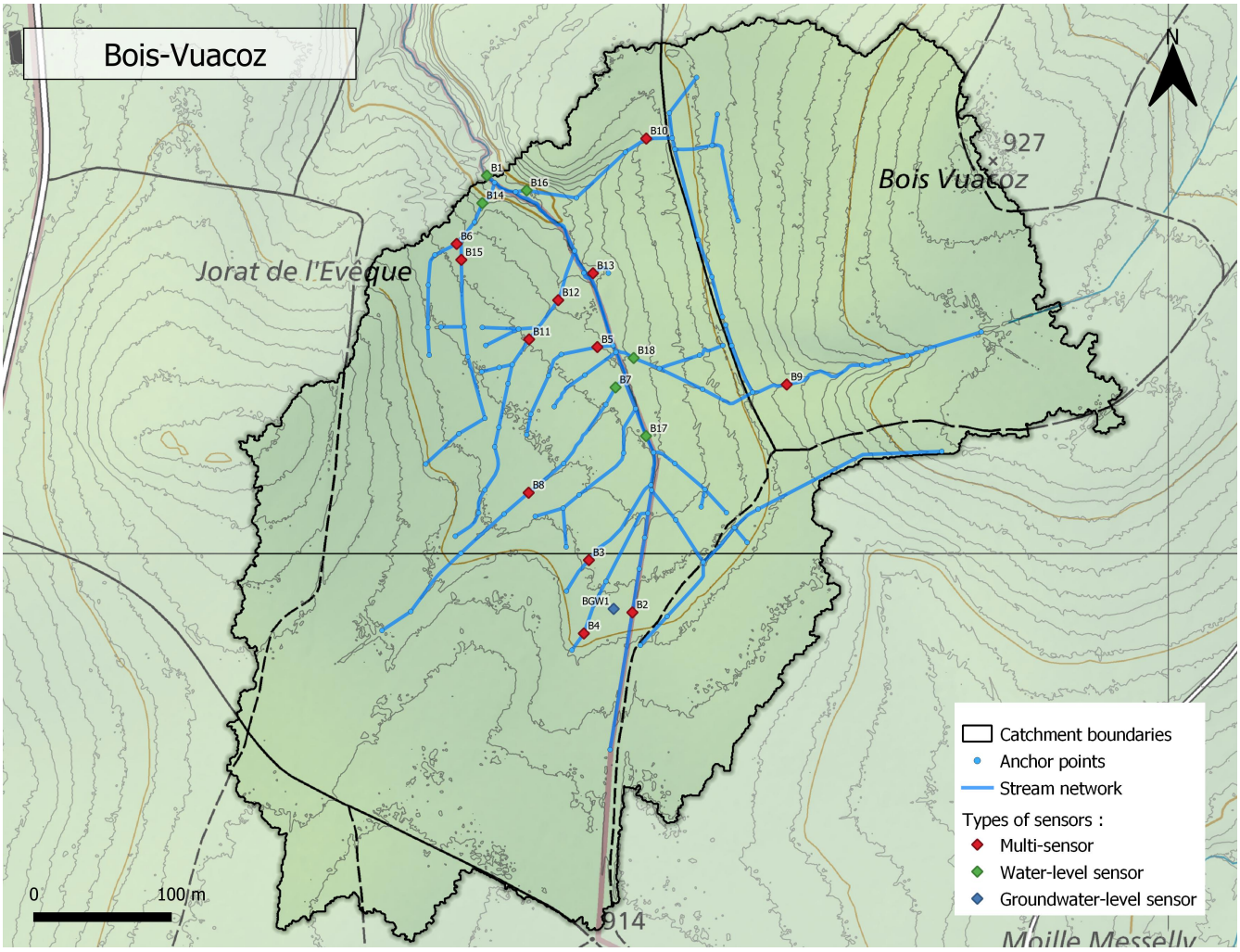

Figure 6: Bois-Vuacoz stream network as a result of catchment mapping. Stream reaches are delimited by geo-referenced anchor points. Monitoring sensors are color-coded according to their type and labelled according to their date of installation. Background map : National map, format 1:10000, by Swisstopo (available on map.geo.admin.ch).

In order to monitor the flowing state of the stream network, I installed a total of 17 sensors distributed among the stream channels : 12 of them were multi-sensors and 5 were water-level sensors. Figure 6 details the position of the sensors.

I used the following criteria to select multi-sensor locations :

- Stream channel width does not exceed 80 cm as we needed to seal the channel bed and banks with a standardised tarp.
- Gradient of slope is greater than 0° as we wanted to ensure a sufficient flow velocity through the impeller in the flow sensor.
- Discharge of the stream does not exceed 120 L/min which is the upper operating discharge for the

flow sensor.

- Stream dries out and wets up regularly as both the ER and flow sensors are made to withstand wetting-drying cycles.

I used the following criteria to determine in-stream locations for water-level sensors :

- Presence of defined cross section with water levels constantly above 2 cm or channel shape allowing for a weir installation.

2.5 Manual water-level and discharge measurements

At every water-level sensor location I measured simultaneously the water-level in the stream and the stream discharge. I read the water-level on a ruler attached alongside the sensor. For the discharge, I used a graduated beaker to collect the entire volume of water flowing through the section during a timed interval. I repeated the operation three times in a row and took the average discharge value.

2.6 Data on mapping surveys

As a part of his semester project, the SIE master student Raphaël Angeles mapped the stream network of Bois-Vuacoz (Angeles 2022). The mapping started on the 1st of March and consisted in covering by foot the whole area of the catchment to identify every geomorphological channel. Angeles divided the channels in stream reaches, i.e., hydrologically homogeneous segments of the stream network and separated by anchor points. Anchor points are precisely geo-referenced physical marks on the terrain. Their numerisation in a GIS application serves to model the stream network. I used data derived from Angeles work.

To conduct my analysis, I used the data collected during four mapping surveys realised the 29th of April, 06th, 13th and 31st of May.

Mapping surveys are snapshots of the hydrological state of the catchment. They have been realised by the SIE student Raphael Angeles as part of his semester project (Angeles 2022), each of them was done within a few hours. He documented the state of every stream segment delimited by anchor points in the network. He used a classification of the stream wetness with 7 levels, from the driest to the wettest : dry stream bed, wet stream bed, standing water, weakly trickling ($\leq$1 L/min), trickling (1-2 L/min), weakly flowing (2-5 L/min) and flowing ($\geq$5 L/min). The result is a detailed list of the hydrological state of each channel segment of the network. As the mapping survey is realised in a few hours, we can assume that the stream states reported by Angeles are all coexisting.

Among the 4 mapping surveys, one dated back to 6th of May, the day after a 10 h long precipitation event. Following this event, the catchment was still wet during the mapping survey. Quite the contrary, the three other mapping surveys captured the progressive drying of the catchment as a rather dry spring

season went on. Capturing the catchment in several hydrological states was important to identify the dynamics of streams activation and deactivation.

2.7 Data processing

2.7.1 Multi-sensor device

Data from the ER and flow sensors are first converted into binary vectors, each bearing a different information on the hydrological state of the stream at the sensor location. For both sensors, the data is transformed into a vector of 1 (presence of water) and 0 (absence of water).

ER sensor The device automatically converts the analog voltage signal recorded between the electrodes of the ER sensor into a digital integer value in the range 0-1023, via an analog to digital converter (ADC). I derived the electrical resistance R in Ohm from the ADC value using equation 1:

$$R = \frac{10000}{\frac{1023}{ADC} - 1} \tag{1}$$

From the data gathered in studies testing and using the same sensors, I used a threshold of 4454 Ω. Values below this threshold indicate a wet stream and values above it indicate a dry stream.

Flow sensor The output of the flow sensor is the discharge in liters per minute. I used the measurement value of 13 L/min as a threshold. Discharge values above 13[L/min] indicate the presence of flow while values below or equal to this threshold signal the absence of flow.

By combining the information carried by both binary vectors, I was able to derive the wetness of the stream at each sensor location and every time-step. Four possible outcomes emerged. They are presented in table 1 :

		Flow state	
		0	1
ER state	0	Dry (0)	Incoherent (-1)
	1	Wet (1)	Flowing (2)

Table 1: Summary of the 4 four possible hydrological states obtained from the combination of the hydrological information derived from ER and flow sensors data.

In addition to the expected dry, wet and flowing states, one outcome emerged several times : an incoherent state. It corresponds to the situation where the flow sensor captured flow while simultaneously the ER sensor records the absence of water.

To resolve this conflict, I performed a visual check of the two time series, plotted together with precipitation and discharge at the outlet in order to detect the source of the measurement error(s). In addition, I used any visual observation of the flow state from the field surveys made at relevant times for the flow state investigation.

Incoherences in the two time series can occur because of :

- Isolated flow spikes detected by the flow sensor (duration of 5 min) in the middle of a dry period : it is possible that the impeller is briefly activated by a gust of wind.
- ER values above the threshold of water detection while water is actually present in the channel : most probably due to limescale building up on the electrodes.
- Flow sensor displaying constant values larger than 13 L/min, seemingly without any responses to actual hydrological variations : found to be linked to a cable disconnected on the breadboard part of the micro-controller board. Flow sensor records could not be used for as long as the problem subsisted.
- After certain rainfall events, the flow sensor measured constant inconsistent values until I performed a sensor check : the problem might come from the impeller.
- Peak discharges sometimes cause the flow sensor to erratically record null values for short periods of time before returning to consistent discharge measurements : I suspect that coarse materials such as leaves and branches mixed with sediments temporarily blocked the entrance of the funnel by forming an impermeable barrier stuck to the mesh protecting the impeller from solid material incursions.
- For small flows, up to 1.5 L/min, the flow sensor approaches its detection limit. At multiple locations and occasions, it failed to detect trickling water.

2.7.2 Water-level sensor

I converted the pressure data returned by the water-level sensors from bar to cm of water column by multiplying it by a factor 1019.72. At this stage, the water-level time series is relative to the position of the sensor measuring head in the water and not the stream bed. In order to obtain the absolute water-level at sensor location, I associated each manual measurement of the water-level, described in 2.5, to the closest sensor measurement in time. For each sensor location, I took the average difference between manual and sensor measurements and added it to the values taken by the sensor. I used between 3 and 4 manual measurement by sensor location to calibrate the time series.

Further cleaning of the data included shifting down a range of values artificially increased by debris either pressing on the measuring head of the sensor or blocking the V-notch used at certain locations.

As for the multi-sensor device, I converted the data from the water-level sensor into a vector containing the hydrological state time series of the monitored location. For this, I determined a discharge threshold of 0.01 L/min. Values above it indicate the presence of flow while values below it are the sign of the absence of flow. I defined this threshold as the tenth of the lowest manual discharge measurement. Indeed, I manually measured a discharge of 0.1 L/min at location B18, on the 27th of May (see 2.5). According to the classification, the stream state was weakly trickling and visually appeared as almost a drop-by-drop. Hence, I made the assumption that a tenth of this value represents flow cessation.

From combined manual water-level and discharge measurements, I derived discharge rating curves : an empirical power-law relationship between discharge and water-level, created for each individual water-level location. Then, I was able to calculate the water-level corresponding to the threshold discharge and distinct water-level from the time series corresponding to the presence of flow (vector = 2) from those corresponding to the absence of flow (wet, 1). Visual observations on the field combined with water-level data visualisation attest that at no point the water-level sensor locations dried up during the monitoring period. Therefore, I did not need to determine a water-level threshold to distinguish between wet state (1) and dry state (0).

2.8 Active stream length and drainage density calculations

To simulate the evolution of the network flowing length, I linked the hydrological behavior of each channel segment to one of the 17 sensor locations.

The four mapping surveys of the stream network contain the hydrological state of each segment of the network at four different dates and therefore at four different catchment wetness conditions. I associated each segment to the sensor location presenting on average the closest hydrological behavior throughout the catchment wetness evolution. I started by applying this methodology to the neighbouring segments of each sensor location. Due to their proximity, I considered these segments more likely to share similar soil characteristics, groundwater table level, average steepness, foliage density, etc. and therefore more likely to exhibit the same hydrological behavior. Then, I applied the same methodology to the remaining segments, not yet attributed to a sensor location. The result can be found in Fig. B.1.

On the 117 segments composing the stream network, I was able to classify 114, i.e. 96.5% of the network length. I did not allocate the remaining 3, as they exhibited a behavior significantly different to any of the sensor locations.

Sensor location	**Length allocated [m]**	**Stream network percentage [%]**
B2	380.91	11.85
B3	181.52	5.65
B4	448.13	13.95
B5	555.58	17.29
B6	326.43	10.16
B7	109.57	3.41
B8	86.08	2.68
B9	147.31	4.58
B10	226.83	7.06
B11	71.87	2.24
B12	37.98	1.18
B13	21.51	0.67
B14	49.23	1.53
B15	14.96	0.47
B16	93.49	2.91
B17	278.76	8.67
B18	69.32	2.16
Not allocated	114.00	3.55
Average	178.53	5.56

Table 2: Details of the stream length and stream network percentage allocated to each sensor location following the method previously detailed. Length measurements have been computed with the software QGIS v.3.16.14-Hannover.

Table 2 details the stream lengths associated with each sensor location and precise what percentage of the stream network it corresponds with. Sensor locations have between 14.96 m and 555.58 m of stream segments allocated to them, for an average of 178.53 m. This represents between 0.47% and 17.29% of the stream network with an average of 5.56%.

Using the segment allocations in combination with the 17 vectors containing the hydrological state at the sensor locations, I calculated the network flowing length every 10 minutes for the monitoring period. The length of every stream segment allocated to a sensor flowing at a given time-step is added. The resulting sum constitutes the stream network flowing length at 10 minutes temporal resolution.

Finally, I determined the drainage density time series by dividing the flowing length by the Bois-Vuacoz catchment area, 25.031 ha.

I assumed the water-level sensor locations B7, B14, B16, B17 and B18 to flow (vector = 2) during the entirety of their respective data gaps. This assumption relies on the presence of flow at these locations at later stages of the monitoring period despite drier conditions. Moreover, I and other operators have observed flow at these sensor locations during each of our visits to the catchment during the periods of data gaps. For the same reasons, I assumed the stream at location B15 to flow between the 22nd and 29th of April, the latter date being the first day with data for this location.

2.9 Empirical relationship between drainage density and catchment discharge

According to (Godsey and Kirchner 2014), a power-law relationship can be observed between drainage density (DD) and catchment discharge (Q), in the form of :

$$DD = \alpha * Q^{\beta} \tag{2}$$

With β in the range [0.18,0.40]. In order to find the best-fitting parameters for the experimental data, the problem can be simplified by transforming 2 into a linear relationship between log(DD) and log(Q).

$$log(DD) = \beta * log(Q) + ln(\alpha) \tag{3}$$

Using Equation 3, a linear regression is performed using the least-square method.

3 Results

3.1 Time series of key hydrological variables

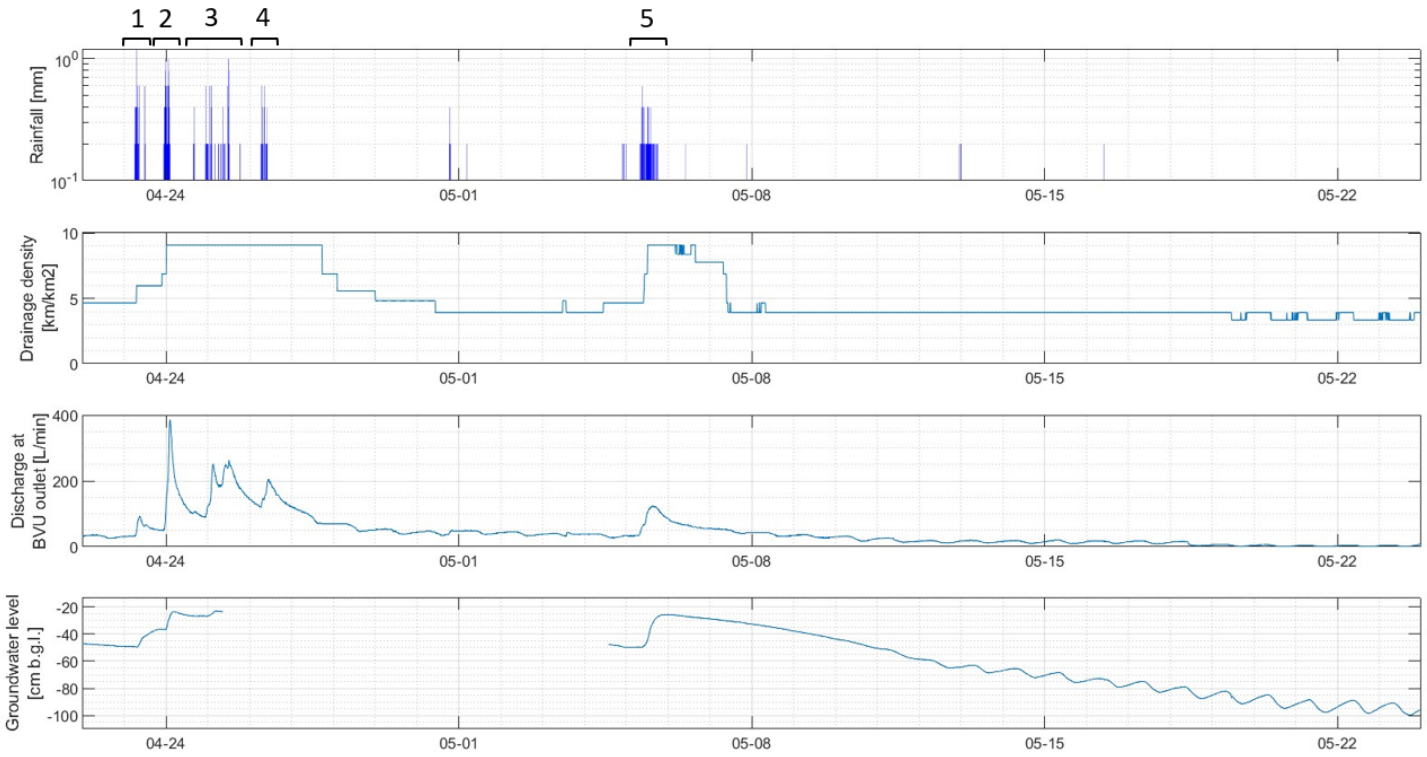

Figure 7: Time series of precipitation, drainage density, discharge at outlet and groundwater level during the monitoring period

Precipitation The top graph of Fig. 7 presents the time series of precipitation during the monitoring period. During the 32 days of the period of interest, rain events occurred on 12 of them. A total of 47.4 mm of rain fell. Two periods appear to be distinctively wet. The first one runs from the 23rd to the 26th of April, lasting 76 h for a total of rainfall measured at 32.8 mm. This period can be subdivided in four rainfall events described in the Table 3 below.

		Duration [h]	Rainfall amount [mm]	Avg intensity [mm/h]	Max intensity [mm/h]
1st wet period	Event n°1	6	7.2	1.2	7.2
	Event n°2	4	10.2	2.6	6
	Event n°3	27	11.2	0.4	6
	Event n°4	3.5	4.2	1.2	3.6
	Period total	76	32.8	0.4	-

Table 3: Rainfall characteristics for every event occurring during the first wet period. Data from Chalet du Villars rain gauge.

The first one, occurred on the 23rd of April. It is closely followed by the second event which straddles the 23rd and 24th of April. Both events are comparable in terms of maximum intensity. The third event is more spread in time with discontinuous raining periods. It started in the middle of the 24th of April and ended in the middle of the 25th of April. The fourth one concerns the 26th of April and is the shortest of the period. Its maximum precipitation intensity is also the lowest of the four.

The second wet period runs from the end of the 04th of May to the end of the 07th of May. Only two significant events occurred during this period. Details can be found in Table 4.

		Duration [h]	Rainfall amount [mm]	Avg intensity [mm/h]	Max intensity [mm/h]
2nd wet period	Event unnumbered	2	0.8	0.4	1.2
	Event n°5	10	11.0	1.1	3.6
	Period total	71	12.2	0.2	-

Table 4: Rainfall characteristics for every event occurring during the second wet period. Data from Chalet du Villars rain gauge.

The first event of the second wet period is both the shortest and the one with the least amount of precipitation (<1 mm) of the six rainfall events described. While the five other events and their effect on the catchment is analysed in the following sections, this event is only mentioned in this section for reasons of completeness. The last event, bearing the number five, is continuous with a long duration. Its maximum intensity is lower compared to events n°1, 2 and 3. The second wet period is both shorter and with a smaller amount of precipitation compared to the first one.

Drainage density The second graph of Fig. 7 represents the computed drainage density for the monitoring period. Two peaks with flat-shaped tops characterise the modeled drainage density time

series.

The first one plateaus for almost 4 days long, at a drainage density of 9.07 km/km^2 which is the maximum value reached in the time series. For the rising limb, the increase happens in two steps coinciding with the times of the first and second rainfall event. Noticeably, the drainage density stays at the plateau during third and fourth rainfall events. Drainage density starts to decrease 31 h after the end of the event n°4, the last of the period. Then, it takes 65 h to fall to the "baseline" value of 3.92 km/km^2.

The second peak reaches a top drainage density as high as the first one but during a much shorter duration. Drainage density starts to increase a few hours after the start of the major rainfall event on the 05th of May and rises faster than the first drainage density peak. The falling limb declines to an intermediary plateau at 7.77 km/km^2 during almost a day before decreasing as steep as the rising limb in a second time. Drainage density starts to decrease 23 h after the end of event n°5. Then it takes 19 h to fall to the "baseline" value of 3.92 km/km^2.

As mentioned, a baseline drainage density, with a value of 3.92 km/km^2 is observed in between the two peaks and after the second one, during drier times. The baseline drainage density starts to contract to 3.33 km/km^2 during day time after staying constant for approximately 12 days in absence of rain.

Discharge at the outlet The third graph of Fig. 7 presents the discharge measured at the outlet of the catchment. Five peaks in the discharge are particularly noticeable. The first four are closely following one another as they happen between the 23rd and 27th of April, i.e. they are the result of the rainfall events n°1-4. The first peak reaches a maximum discharge of 91.74 L/min. The second one has a sharp appearance and is distinctively higher than the other ones. At its maximum, the discharge is 384.61 L/min. The third peak is shaped differently. This time the summit of the peak can be subdivided in three different high points. The first and last of these high points are separated by 9 h. While it never goes above a discharge value of 263.54 L/min, this peak duration is significantly longer than the first and second ones. The fourth peak tops at a discharge of 204.14 L/min. Each one of these peaks starts at a discharge value higher than the precedent one.

Following these peaks, a period of lower discharge occurs between the 27th of April and 04th of May, because of a lack of precipitation. During this time, the overall trend is a slow decrease in discharge accompanied by slight discharge oscillations with a period close to 24 h.

The fifth peak starts on the 05th of May, the same day as a rainfall event previously described. Its peak has a rounded shape as opposed to the sharper shape of other event peaks.

After the fifth peak, a second period of lower discharge starts around the 08th of May. This time again, a trend of slow decrease in discharge accompanied by daily oscillations is noticeable. From the 18th of May to the end of period, discharge stays constantly below the 10 L/min mark, reaching the lowest value of 0.66 L/min.

Rising and falling limbs are asymmetrical for the discharge of every rainfall event, with a much steeper

increase.

Groundwater level The last graph of Fig.7 is the time series of the groundwater level measured at the location BGW1. A period of time running from the 25th of April to the 04th of May lacks data recording due to the technical difficulties. This represents almost 29% of the monitoring period. Before the interruption of the time series, three peaks can be observed. As for the discharge, these peaks happen approximately at the same time as the rainfall events. However their shape is differs from the previously described peaks. In particular the second one shows a rapid rise of the groundwater level followed by a very slow groundwater level decrease.

On the 05th of May, an other peak arises and this time, as the series of value is not interrupted, both limbs can be clearly described. The rising limb presents a steep and steady increase of the groundwater level, which ends in a rounded top. The falling limb shows a very slow decrease of the groundwater level with a slightly convex shape. This indicates that the water table recession accelerates progressively as it gets lower. The end of the falling limb is hardly noticeable as the groundwater level continues to decrease until the end of the period scrutinized. Nonetheless, around the 11th of May, the convex behavior is replaced by an oscillation whose period is around 24 h and its amplitude progressively increase.

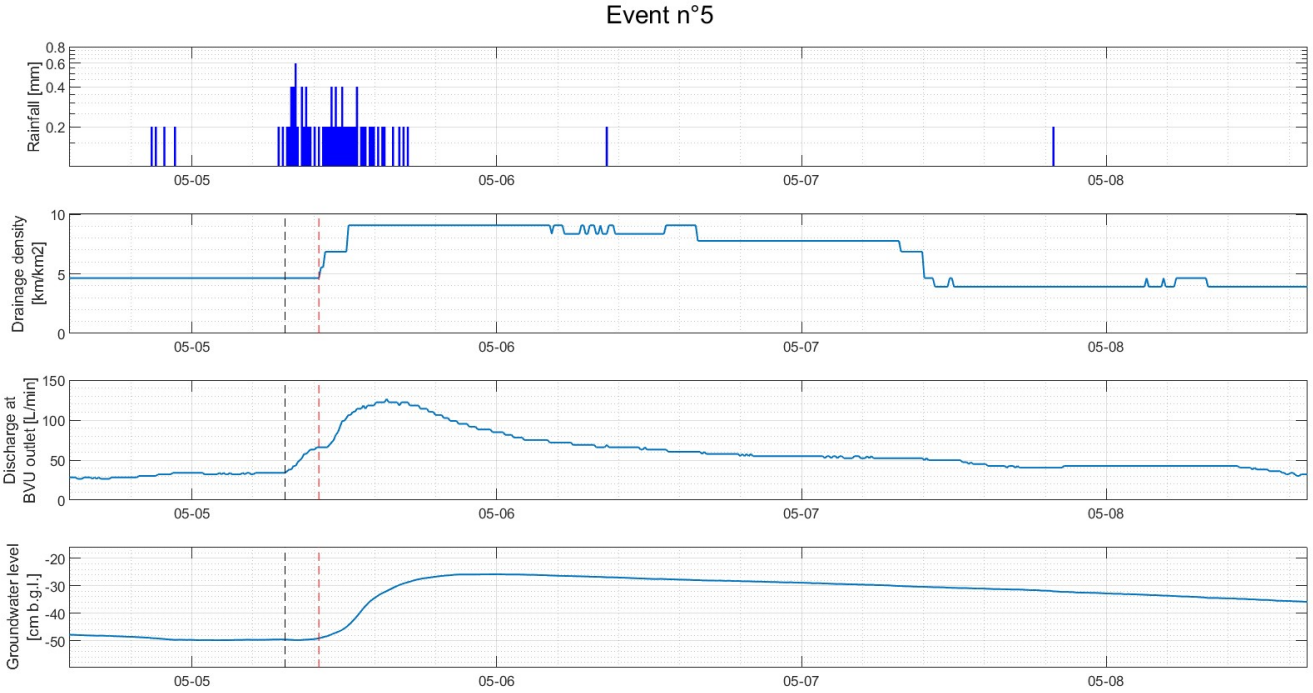

Figure 8: Time series of precipitation, drainage density, discharge at outlet and groundwater level for rainfall event n°5. The black dashed line points the start of the discharge increase while the red dashed line indicates the start of the drainage density and groundwater level increase.

Figure 8 focuses on the interval time surrounding the rainfall event n°5.

The black dashed line indicates the time at which the discharge increase begins (3rd panel). At this moment, both the drainage density and the groundwater level are still small (2nd and 4th panels). The red dashed line points the instant at which the drainage density and the groundwater start to rise. Black and red lines are separated by 3 h although rain fell during this entire period.

Noticeably, the discharge rising limb is composed of two steps. The first one occurs before drainage density and groundwater level begin to increase. The second one is simultaneous with the drainage density and groundwater level rising limbs.

3.2 Relationship between drainage density and discharge measured at outlet

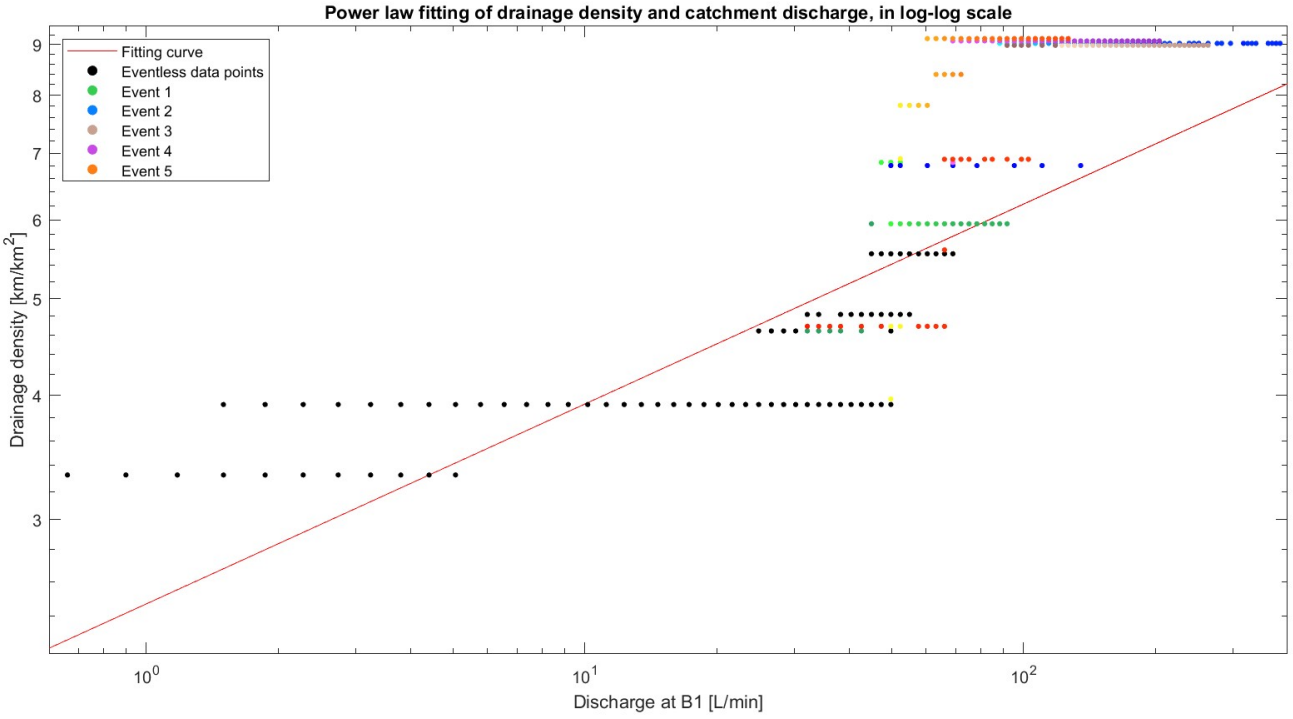

Figure 9: Log-log plot of the the modelled power-law relationship between drainage density and catchment discharge. Points from the data set are color-coded according to their belonging to a rainfall event. Overlapping data points from different events have been slightly vertically shifted to help their differentiation.

Figure 9 presents the the power-law fitting of the computed drainage density to the discharge measured at the outlet.

Values of the parameters for the fitted power-law are $\alpha = 2.47$ and $\beta = 0.20$. As the fitting has been performed using a linear regression, the coefficient of determination is 0.57. The visualisation of the fitted curve is realised in log-log scale in order to simplify the visual analysis.

Noticeably, the fitting of the power-law to the data set does not seem accurate. Indeed, as the discharge

increases, the experimental drainage density clearly seems to curve upward, creating a clear offset between high discharge data points and the fitted linear regression. At the upper end of this curve, the drainage density reaches a plateau at 9.1 km/km^2, the highest registered value during the monitoring period. From this point, any increase in the discharge value does not translate in an increase of the drainage density.

From 0.7 L/min, the smallest value of discharge observed, to approximately 20 L/min, the drainage density appears to vary only slightly from 3.3 to 3.9 km/km^2. The slope of this subset of data points is visually lower than the linear regression one. Then, for discharges from around 20 to 100 L/min, the drainage density rises from 3.9 to 9.1 km/km^2, an increase much faster than the linear regression. It can be observed that data points captured during periods characterised by the absence of rainfall events (represented in black) and those captured during rainfall events (represented in colors) form two different clusters on the graph. The former contains the lower half of drainage density values (between 3 and 6 km/km^2) and the lowest discharges (inferior to 100 L/min) while the latter encompasses the higher half of drainage density values (between 6 and 9 km/km^2) and discharges varying over a greater range, going from 100 to almost 400 L/min.

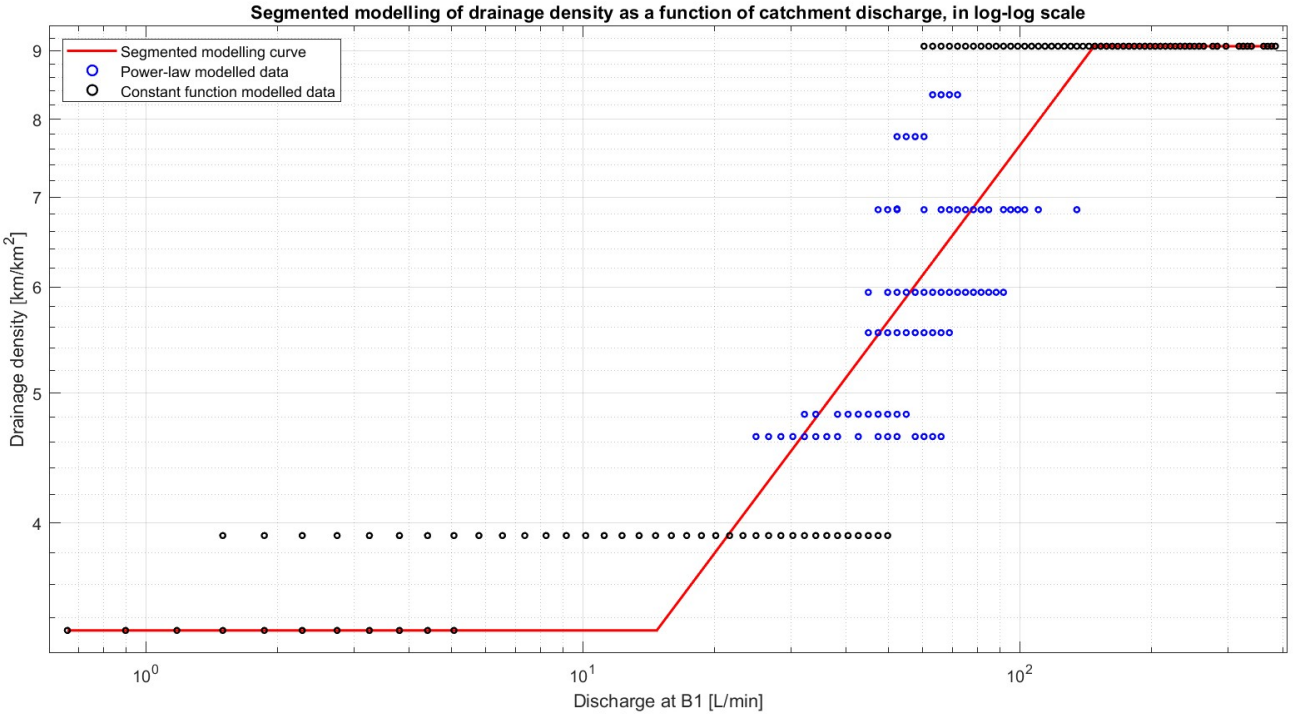

Figure 10: Log-log plot of the segmented modelling of the relationship between drainage density and catchment discharge. Drainage density minimum and maximum boundaries are represented as constant functions in red. Corresponding subset of data is in black. Power-law relationship for subset of data where the drainage density is in between the boundaries is in red. Corresponding subset of data is in blue.

The Fig. 9 showed that a power-law model lacks some complexity to represent the boundaries observed at low and high drainage densities. In order to correctly model the different phases of the relationship between drainage density and discharge, I divided the modelling curve in three segments (see Fig. 10).

The first and third segments are constant functions. They model the min and max boundaries observed in the computed drainage density. The first constant function is the minimum drainage density 3.33 km/km^2. It starts from the lower observed discharge and joins the second modelled segment at a discharge of 14.7 L/min. The other constant function is the maximum drainage density 9.07 km/km^2. It starts at the end of the second segment at a discharge of 148.5 L/min and ends at the maximum observed discharge. In between these segments, the second segment is a modelled power-law. The subset of data (in blue) used to fit the model is only composed of data points that are in between the drainage density boundaries, i.e. with drainage densities in the range 4.64-8.39 km/km^2. It corresponds to the points where the drainage density is positively correlated with the discharge.

The resulting model takes into account the separate phases of the relationship between drainage density and discharge. The fitted power-law more accurately represents the data compared to Fig. 9. The β-parameter is equal to 0.44, underscoring the correlation between drainage density and discharge for drainage densities in between the min and max boundaries. The coefficient of determination for the linear regression used to compute the power-law has a value of 0.50. The sharp junctions between the three modelled segments do not accurately represent the progression from one phase to another between drainage density and discharge.

3.3 Relationship between drainage density and groundwater level

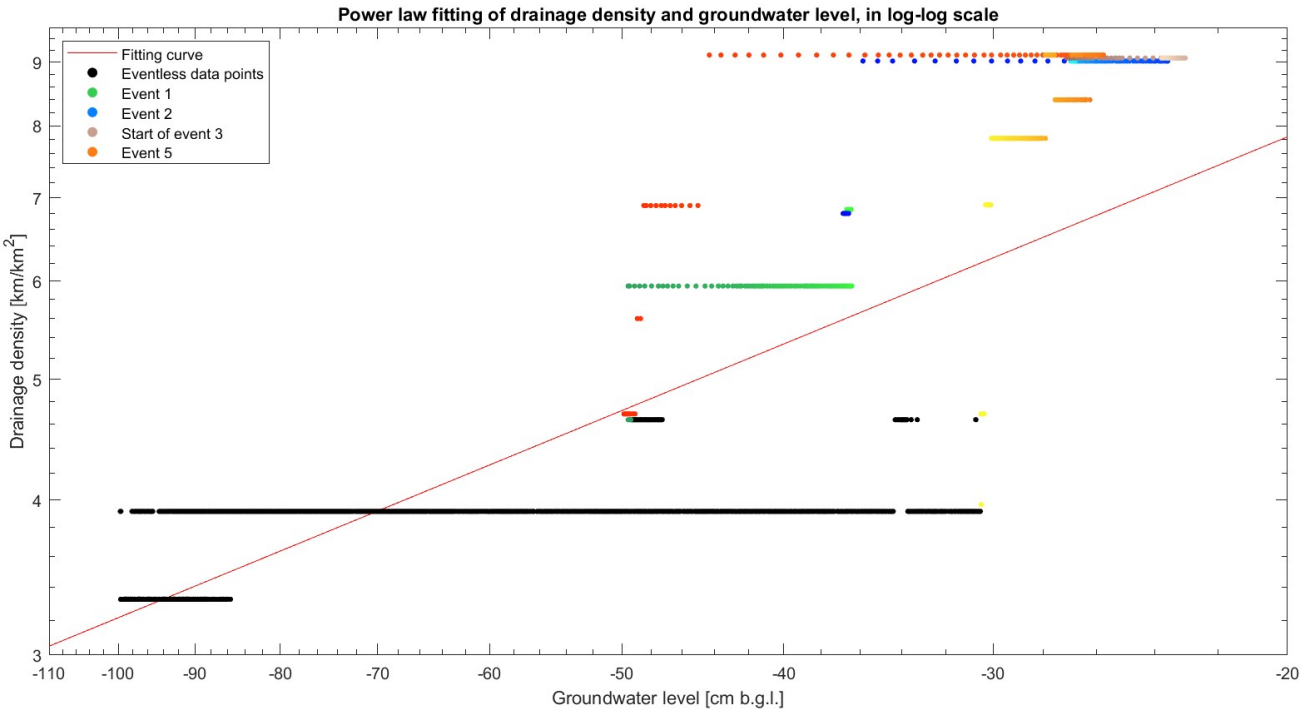

Figure 11: Log-log plot of the the modelled power-law relationship between drainage density and groundwater level. Points from the data set are color-coded according to their belonging to a rainfall event. Overlapping data points from different events have been slightly vertically shifted to help their differentiation.

Figure 11 presents the fitting of a power-law between the computed drainage density and the measured groundwater level in the catchment.

Due to the gap in data collection of the groundwater level, only two third of the monitoring period is used to perform the power-law fitting. While rainfall events n°1, 2 and 5 have been entirely recorder by the groundwater level measuring sensor, event n°3 is missing most of its development and event n°4 is completely absent.

As in the previous power-law fitting, between drainage density and discharge, the modelled curve does not accurately represent the shape of the data set. Several features acknowledged in the description of figure 9 are present as well in figure 11. Indeed, for low groundwater levels, between -100 cm b.g.l. and -50 cm b.g.l., a large concentration of data points are contained in a small range of drainage densities, between 3.3 and 3.9 km/km^2. All of them belong to periods characterised by the absence of rainfall event (represented in black). Furthermore, a drainage density of 3.9 km/km^2 has been found to correspond to groundwater levels ranging from -100 to -30 cm b.g.l., that is to say over 90% of the recorded range of variation of groundwater level during the monitoring period. In parallel, a groundwater level of -30 cm b.g.l. has been linked to drainage densities ranging from 3.9 to 9.1 km/km^2, covering approximately 90%

of the computed range of variation of drainage density.

These particular numbers highlight two features of the relationship between drainage density and groundwater level. In first, the lack of response to groundwater level variations for low drainage densities during periods without rainfall events and in second the noticeable positive correlation between both variable at higher ranges, for which most of the data points were captured during rainfall events. This correlation has a greater slope than that of the linear regression (in log-log representation).

Another feature already observed in figure 9, is the plateau reached by the drainage density, which extends from groundwater level of -45 cm b.g.l. to the maximum observed value of -23 cm b.g.l. .

A small part of the subset of data points belonging to periods without rainfall events (represented in black) have a distinctively higher drainage density than the rest of the subset. Their drainage density is close to 4.6 km/km^2. One part corresponds to the short time interval between the start of the monitoring period and the beginning of the first rainfall event and the other part corresponds to the brief time span between the end of the data gap and the start of the fifth event. For the latter, the absence of groundwater level measurements prior to the selection of points make it hard to put them in perspective.

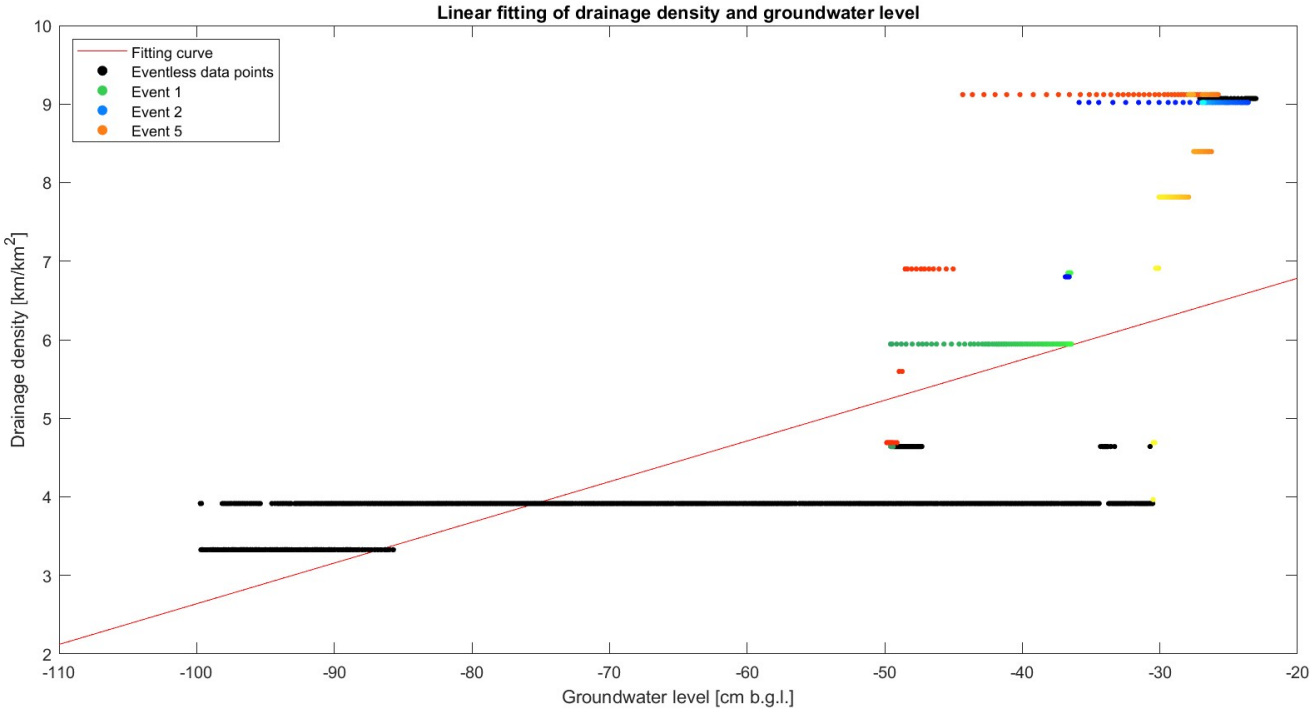

Figure 12: Plot of the the modelled linear relationship between drainage density and groundwater level. Points from the data set are color-coded according to their belonging to a rainfall event.

Figure 12 represents the modelled linear regression fitted between drainage density and groundwater level. Most of the descriptive comments made on the fitted power-law between drainage density and

groundwater level, Fig. 11, remain valid to describe the fitted linear regression between the same variables, see Fig. 12.

Visually, the fitted curve does not accurately represent the data set. The model does not capture the plateaus observed at low and high drainage density. Moreover, the slope of the linear regression fails to match the actual slope of the subset of data captured during precipitation periods with a drainage density inferior to the upper-limit.

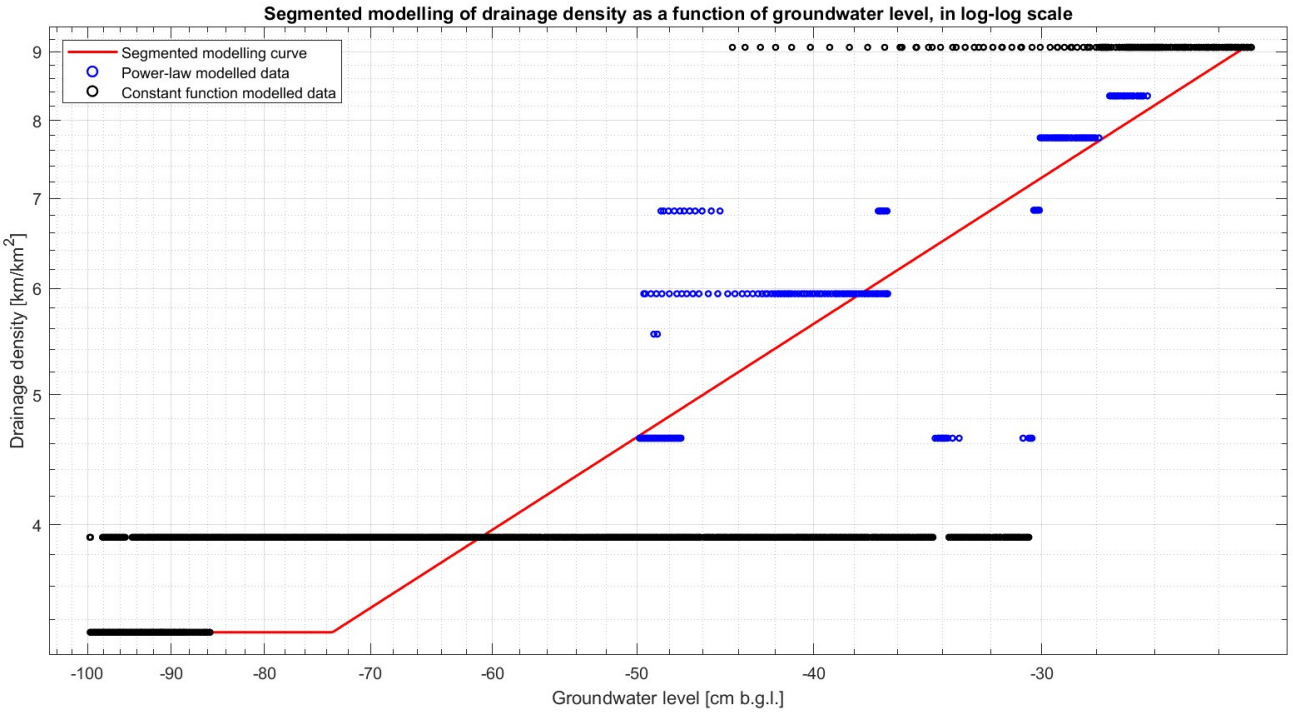

Figure 13: Log-log plot of the segmented modelling of the relationship between drainage density and groundwater level. Drainage density minimum and maximum boundaries are represented as constant functions in red. Corresponding subset of data is in black. Power-law relationship for subset of data where the drainage density is in between the boundaries is in red. Corresponding subset of data is in blue.

The Fig. 11 and 12 showed that a power-law function or a linear regression are not able to model the boundaries observed at low and high drainage densities. Following the method used to model the relationship between drainage density and discharge, I divided the modelling curve in three segments (see Fig. 13).

I used two constant functions to model the min and max boundaries of the drainage density. The first constant function, with a value of 3.33 km/km^2, starts at the minimum observed groundwater level and joins the second segment at a groundwater level of -73.4 cm b.g.l. . The other constant function, with a value of 9.07 km/km^2, follows the second segment, starting at -23.2 cm b.g.l. and ending at the maximum

observed groundwater level -23.0 cm b.g.l. . In between these segments, the data (in blue) showing a positive correlation between drainage density and groundwater level is modelled by a power law function.

The subset of data composing the minimum boundary (in black) ranges from -100 to -30 cm b.g.l. and greatly overlap with the subset of data used to model a power law (in blue). Hence, the groundwater level of -73.4 cm b.g.l. at which the two functions intersect does not accurately represent the transition from the minimum drainage density boundary to the increase drainage density phase. The same problem occurs with the maximum boundary. The overlap between the black and blue subset of data is so important that the power-law and the constant functions intersect at only 0.2 cm from the maximum groundwater level. The coefficient of determination for the linear regression used to compute the power-law has a value of 0.79.

3.4 Drainage density variations during rainfall events

To address the third research question, I computed for each rainfall event identified the antecedent wetness, calculated as the quantity of water fallen onto the catchment in the previous 72 h before the start of the event.

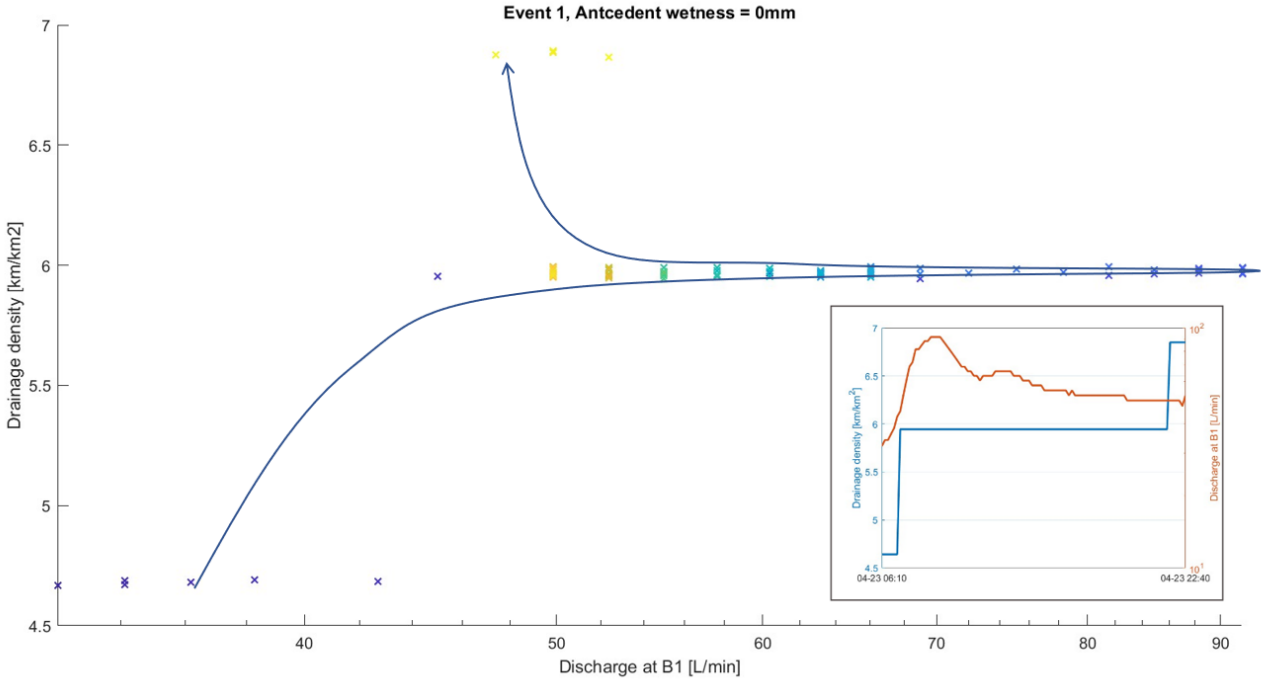

Figure 14: Drainage density as a function of discharge at the outlet, during rainfall event n°1. Time direction is indicated by arrow and color variation : from dark blue to yellow. Vertical jittering has been introduced to distinguish overlapping points from different times. In insert, time series of the drainage density and discharge during the same period.

Event n°1 The first event, presented in Fig. 14, has an antecedent moisture of 0 mm and a total precipitation of 7.2 mm. At first, the logarithm of discharge increases from 32 to 91.7 L/min before

decreasing around 47.4 L/min at the moment where the second rainfall event starts. During the same interval, the drainage density constantly increases from 4.6 to 5.9 km/km^2.

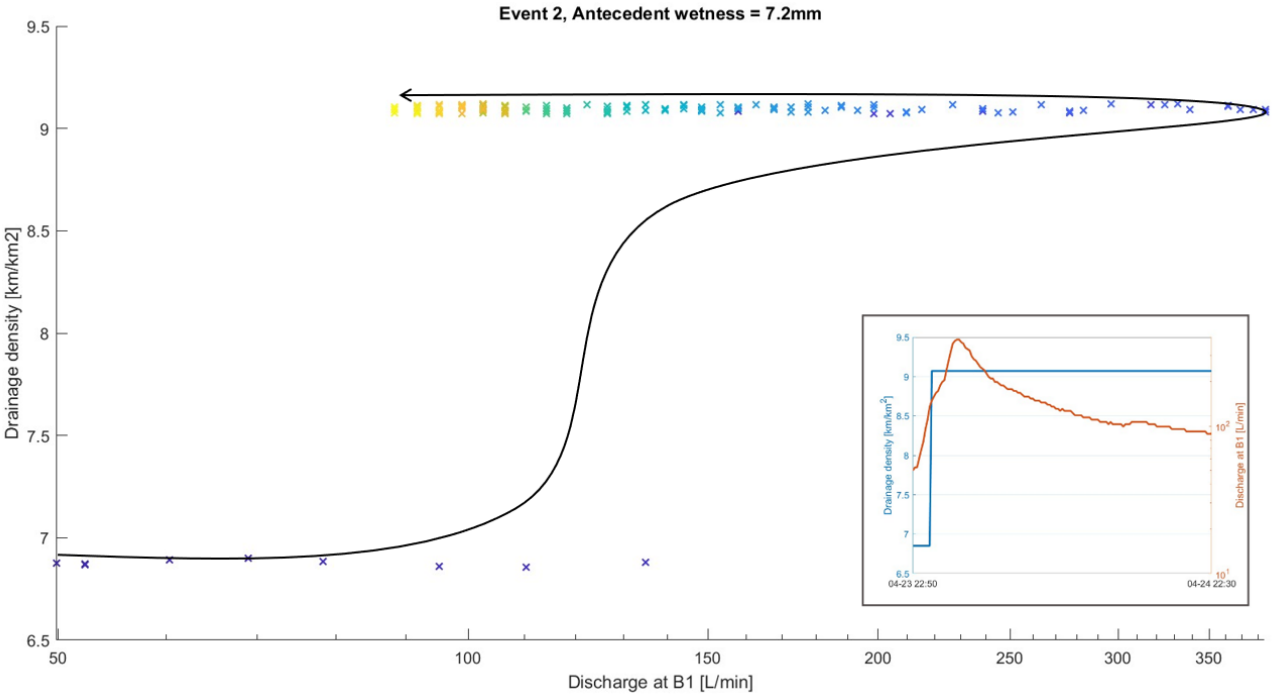

Figure 15: Drainage density as a function of discharge at the outlet, during rainfall event n°2. Time direction is indicated by arrow and color variation : from dark blue to yellow. Vertical jittering has been introduced to distinguish overlapping points from different times. In insert, time series of the drainage density and discharge during the same period.

Event n°2 The second event, presented in Fig. 15, starts immediately after event 1. It has an antecedent moisture of 7.2 mm and a total of precipitation of 10.2 mm. During this event, the logarithm of discharge increases from 49.8 to 384.6 L/min before decreasing to 88.2 L/min when the third event starts. On the same time, the drainage density increases from 5.9 to 9.1 km/km^2 where it plateaus.

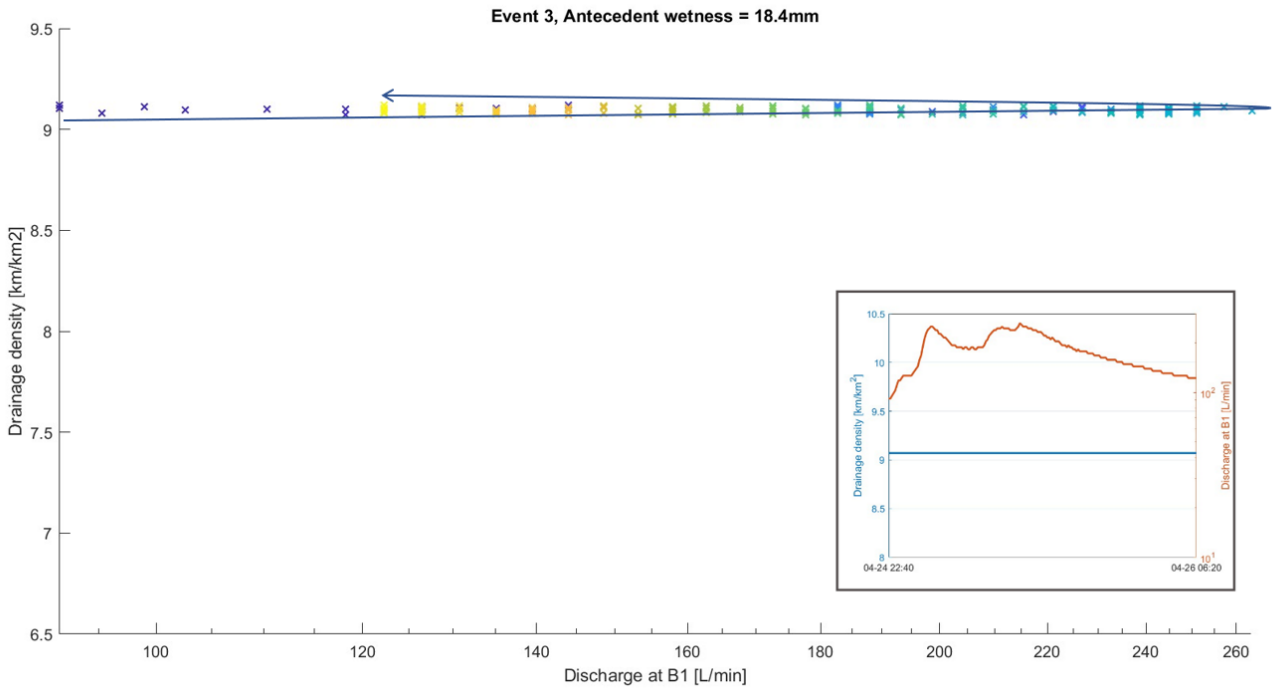

Figure 16: Drainage density as a function of discharge at the outlet, during rainfall event n°3. Time direction is indicated by arrow and color variation : from dark blue to yellow. Vertical jittering has been introduced to distinguish overlapping points from different times. In insert, time series of the drainage density and discharge during the same period.

Event n°3 The third event, presented in Fig. 16, follows immediately the second one. Its antecedent moisture is 18.4 mm and the amount of precipitation falling is 11.2 mm. As for previous rainfall events, discharge first increases from 91.7 to 263.5 L/min before decreasing to 122.3 L/min when the fourth event begins. However, this time, the drainage stays at constant value of 9.1 km/km^2 which corresponds to the plateau reached during most of the second event and also the maximum discharge density computed during the analysis period.

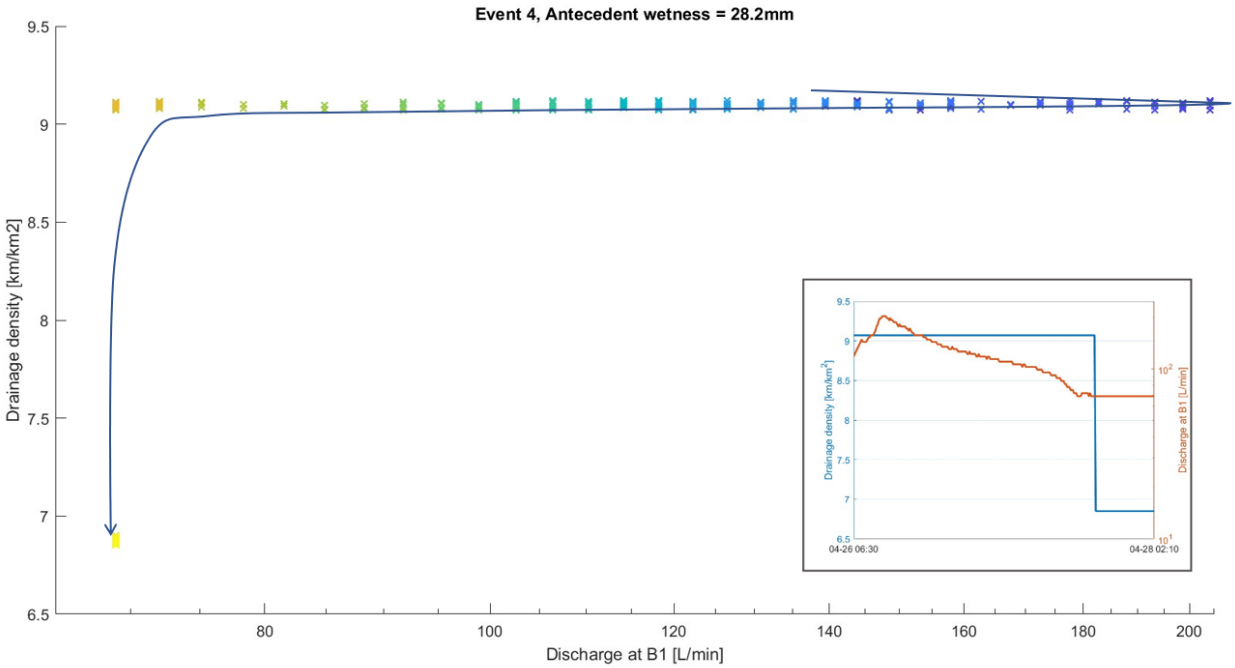

Figure 17: Drainage density as a function of discharge at the outlet, during rainfall event n°4. Time direction is indicated by arrow and color variation : from dark blue to yellow. Vertical jittering has been introduced to distinguish overlapping points from different times. In insert, time series of the drainage density and discharge during the same period.

Event n°4 The fourth event, presented in Fig. 17, is the last one of the continuous series of rainfall events. At this point, the antecedent moisture is 28.2 mm. The total amount of precipitation during this event is 4.2 mm. The discharge increases from 118.2 to 204.1 L/min before decreasing to 69.0 L/min. As, this event is last of the series, it includes not only the falling limb but also the complete recession, a longer period of time during which the discharge has the time to decrease to lower levels. As a result, unlike the three precedent events, the ending discharge is lower than the starting one. The drainage density stays constant during the major part of the event at 9.1 km/km^2, the value observed in events n°2 and 3, before lowering around 6.9 km/km^2 at the end.

Another way to define the boundaries for this event could be to extend it for one day. In this case, the ending drainage density would lower to 4.8 km/km^2, a value much closer to the one at the start of event n°1.

Rainfall events n°1 to 4 follow each other. An individual description of each event brings a partial information. One gains more insights by analysing the response of drainage density and discharge on a time-scale encompassing the four events :

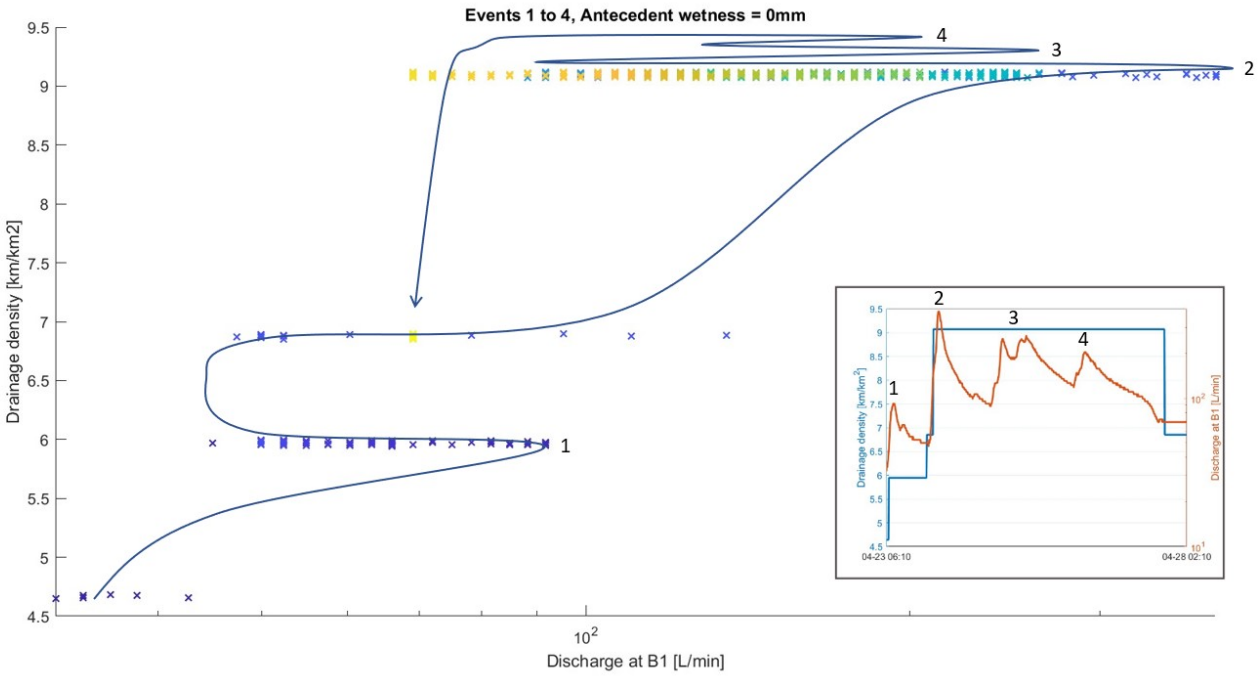

Figure 18: Drainage density as a function of discharge at the outlet, during rainfall events n°1 to n°4. Events are numbered in the figure. Time direction is indicated by arrow and color variation : from dark blue to yellow. Vertical jittering has been introduced to distinguish overlapping points from different times. In insert, time series of the drainage density and discharge during the same period.

Events n°1 to n°4

In Fig. 18, the general shape of the plot is an approximate counter-clockwise loop with its ending side (in yellow) not fully closing the loop. Most of the drainage density variations happen in the initial and closing phases of the period. Indeed, the drainage density reaches its upper-limit soon after the start of the second event and only initiates a recession after the end of the last event discharge falling limb. On the other hand, the discharge experiences a succession of rises and falls during the entire period.

Noticeably, during event n°2, the drainage density reaches its upper-limit value a few hours before the discharge peaks. Furthermore, for each event it clearly appears that the drainage density is able to maintain its peak level for periods of time of the order of days after the discharge enters in recession.

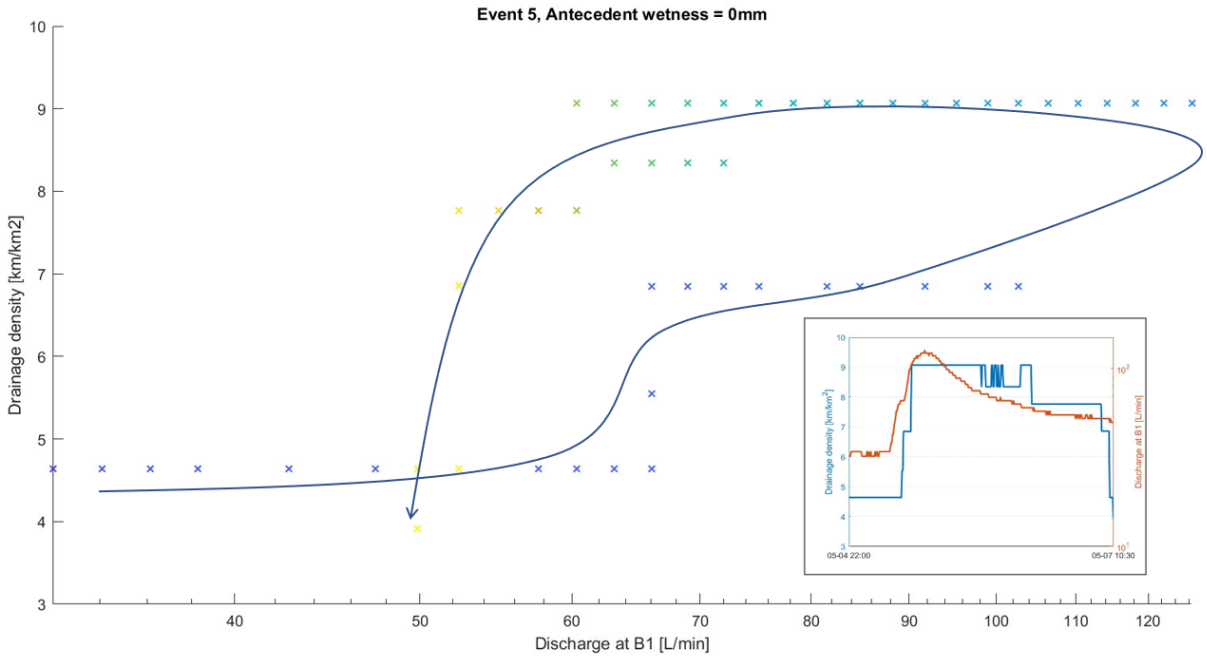

Figure 19: Drainage density as a function of discharge at the outlet, during rainfall event n°5. Time direction is indicated by arrow and color variation : from dark blue to yellow. In insert, time series of the drainage density and discharge during the same period.

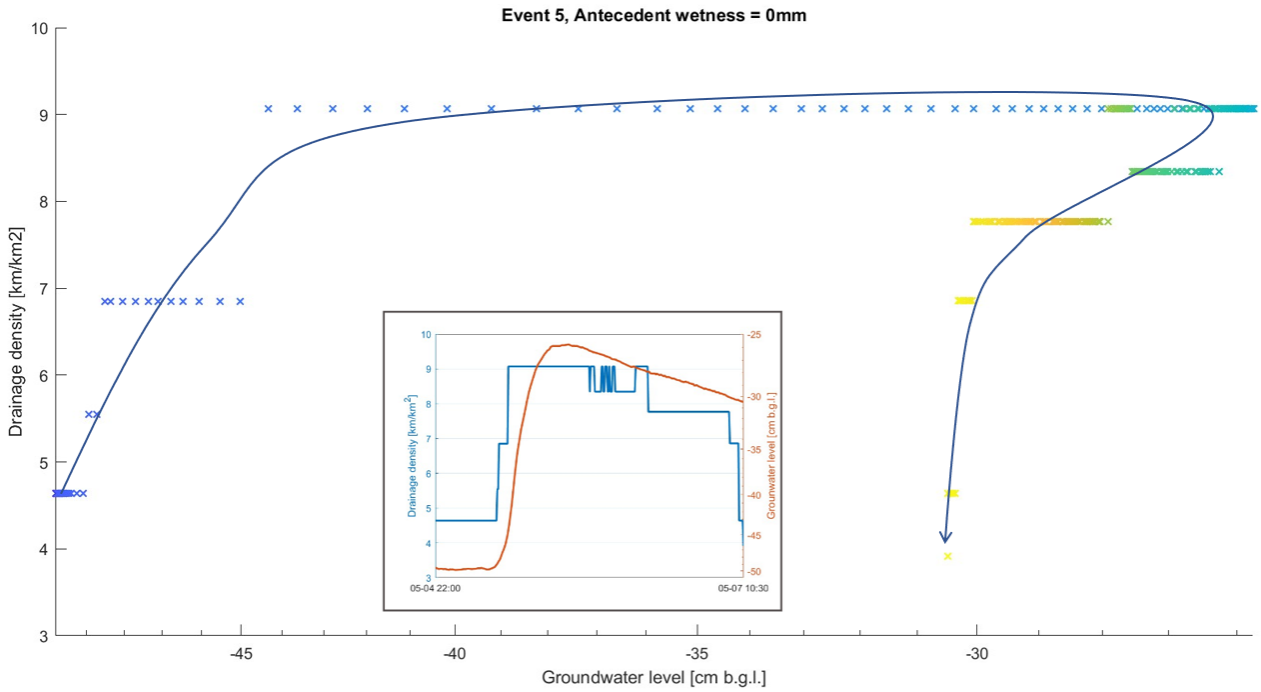

Figure 20: Drainage density as a function of groundwater level, during rainfall event n°5. Time direction is indicated by arrow and color variation : from dark blue to yellow. In insert, time series of the drainage density and groundwater level during the same period.

Event n°5 The fifth event, presented in Fig. 19 took placed during the wet period in May. It is characterised by an antecedent moisture of 0.8 mm and a total amount of precipitation of 11 mm. The discharge first rises from 32.1 to 126.4 L/min before decreasing to a value of 49.8 L/min. The drainage density is first on an upward trend followed by a downward one, going from 4.6 to 9.1 km/km^2 then to 3.9 km/km^2. The maximum drainage density reached is the maximum one overall, which also has been achieved during events n°2,3 and 4.

The data points form a counter-clockwise loop. That is to say, for a given value of discharge reached both during increasing and decreasing phases of the event, the corresponding drainage density values are different: the latest (decreasing phase) being superior to the other one (increasing phase).

In Fig. 20, where drainage density is plotted against groundwater level, the data set almost forms a clockwise loop. For equal values taken by the drainage density during rising and falling phases, the groundwater level is close to be 20 cm higher in the latter phase.

3.5 Spatio-temporal patterns in stream activation

To address the first research question I calculated for each sensor location, the vector summarising the state of the stream during the monitoring period is used to compute the percentage of time the stream reaches allocated to the location have spent activated.

Sensor location(s)	**Persistency** [%]	**Flowing stream network length** [%]
B7/B8/B11/B12/B13 B14/B15/B16/B17/B18	100.0	25.92
B9	90.9	4.58
B3	30.7	5.65
B10	26.6	7.06
B6	18.8	10.16
B5	17.5	17.29
B2/B4	0.0	25.80

Table 5: Calculation of the flow persistency in time per sensor location. Sensor locations with the same persistency are grouped together. Percentage of the stream network corresponding to each persistency level is added.

Table 5 shows the percentage of time sensor locations and their allocated stream reaches are activated and the percentage of stream network concerned, per sensor location. Interestingly, the stream reaches which remained always activated and the ones which never activated comprise each almost 26% of the stream network. 40% of the stream network length is constituted of stream reaches with a persistency in the range 17.5-30.7% while no stream reach have a persistency in the range 30.7<[...]<90.9, i.e. a 60.2% gap in observed persistency levels.

Stream reaches are ranked and color-coded by their persistency. A map of the stream network is created to observe the spatio-temporal patterns in stream activation.

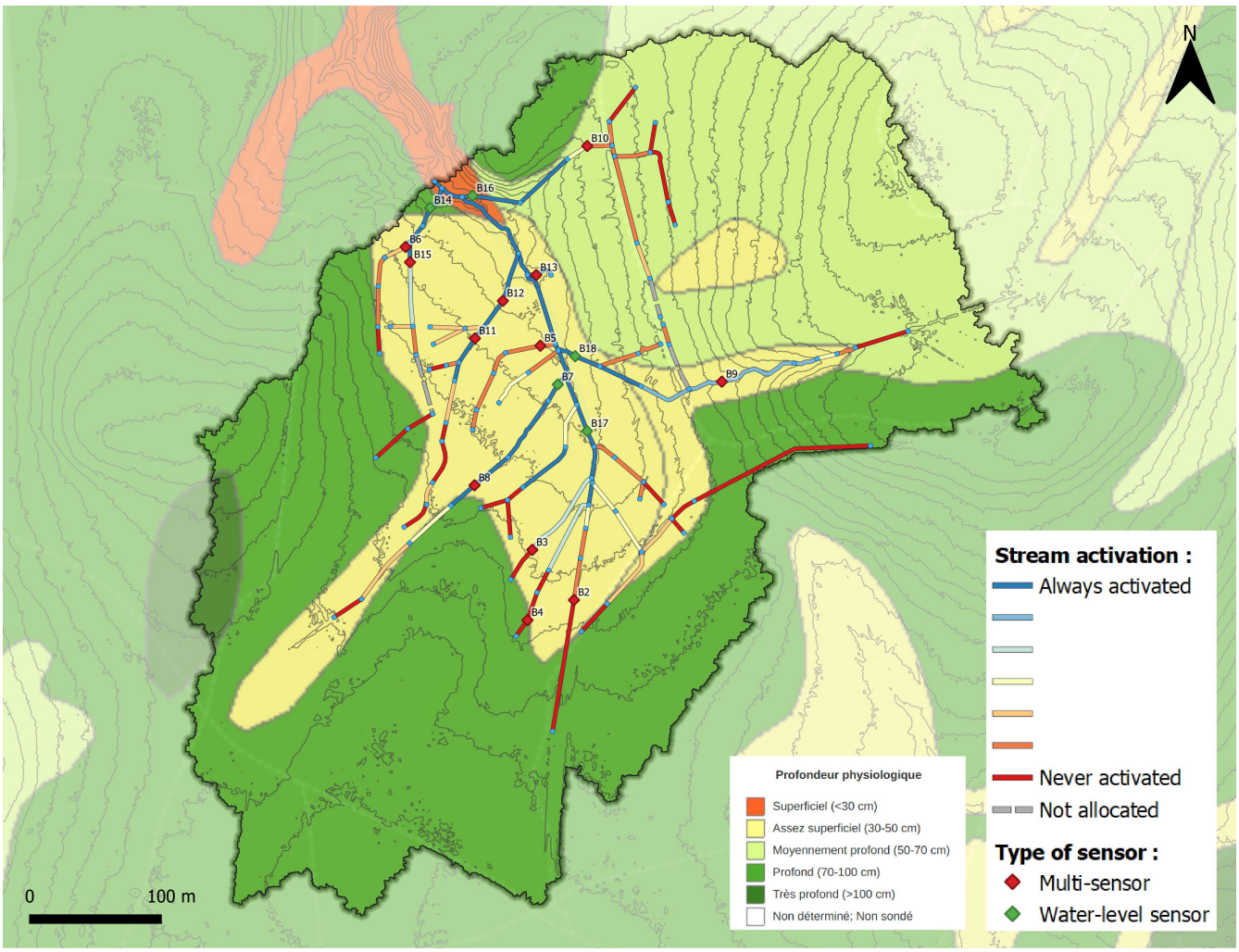

Figure 21: Stream network color-coded by flow persistency in time. Background map is physiological depth of the soil, layer from geo.vd.ch. Physiological soil depth is color-coded as follows : superficial (<30 cm) in red, fairly superficial (30-50 cm) in yellow, moderately deep (50-70 cm) in light green, deep (70-100 cm) in green, very deep (>100 cm) in dark green, absence of data in white

Figure 21 superimposes the stream network color-coded by persistency and a background map of the catchment physiological soil depths.

The main stream corresponds to the the central channel of the stream network, with a persistency of 100%. Along its course to the outlet, it drains 13 tributary streams.

Six of the tributary streams sharing a junction with the main stream also have a persistency of 100%. A seventh, tributary stream contains a reach with a persistency of 100% but at its junction with the main stream, its flow persistency is much lower.

A vast majority of the stream heads mapped have a null persistency over the course of the monitoring period. Tributary streams with a length <100 m are the only ones that only contain stream reaches with persistency greater than zero.

Superimposed to the stream network is a map of the soil physiological depth in the catchment. Superficial soils with a depth smaller than 30 cm are only found around the outlet of the catchment. They include the northernmost reaches of the main stream as well as the junctions with two tributary streams. Fairly superficial soils, with a depth between 30 and 50 cm occupy the central low-land area of the catchment and encompass most segments of the stream network including the main stream. Most of the flowing segments are in this area of the catchment. Moderately deep and deep soils with respective depths ranging from 50 to 70 cm and 70 to 100 cm surround the fairly superficial soils and occupy the upper-lands of the catchment.

On the western and southern parts of the catchment, only the head of several streams are on deep soils. All of them stayed deactivated during the entire monitoring period. Along the eastern part of the catchment, more stream segments can be found on deep and moderately deep soils. While the heads of these streams did not activate during the monitoring period, several segments up- and down-stream B10 have been activated.

Interestingly, most of the segments found on deep and moderately deep soils, in particular upstream B2 and the branching at the east of B2 as well as the segments upstream B10, are man-made. The presence of channels at these locations is not the result of the local geomorphological and hydrological conditions.

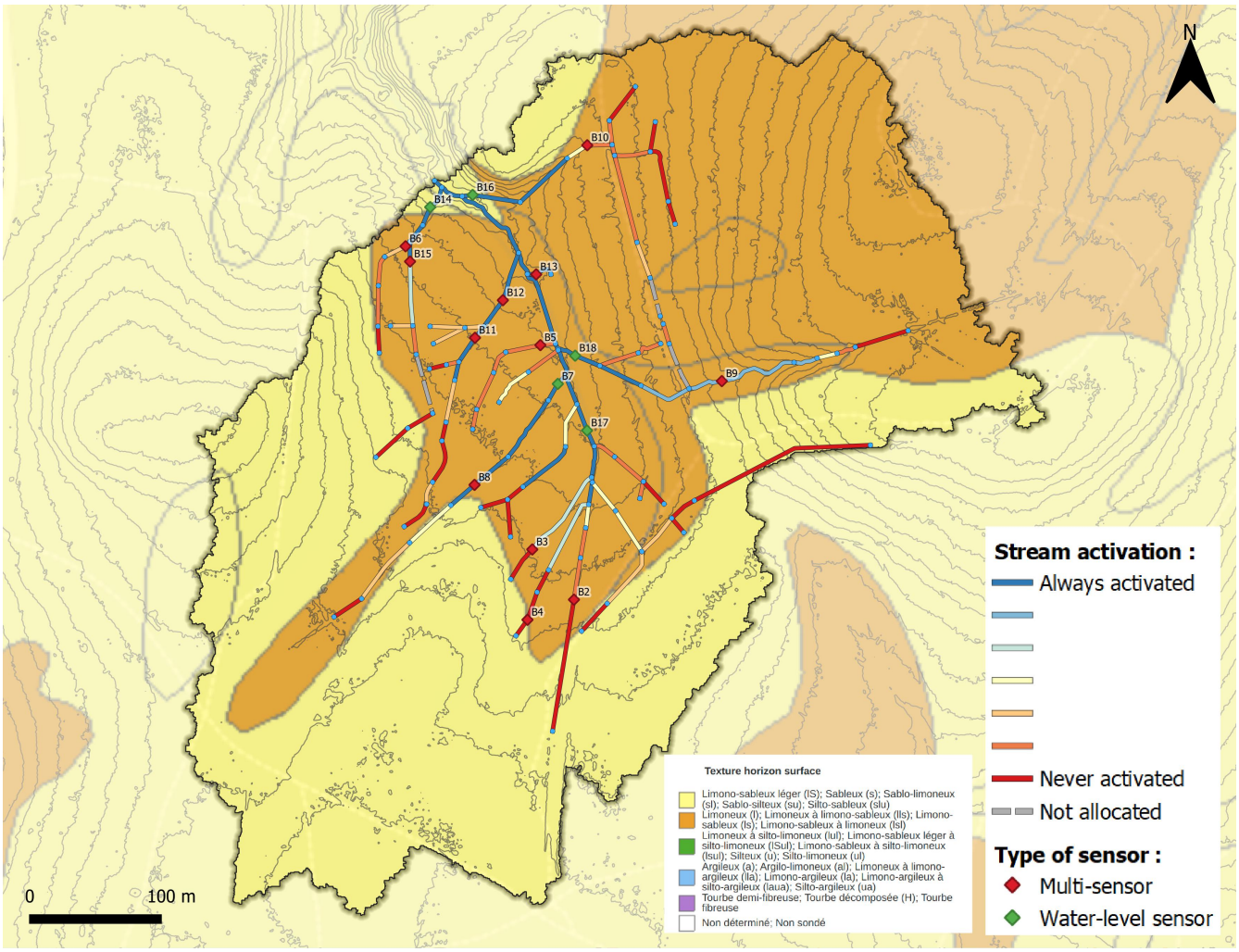

Figure 22: Stream network color-coded by activation time and surface horizon texture, layer from geo.vd.ch. silty/sandy-silty surface horizon is in orange and light sandy-silty layer is in yellow.

Figure 22 is a map of the surface horizon texture with a superimposition of the stream network ranked by stream activation time. Soil texture refers to the composition of its mineral fraction, i.e. in which proportions we find sand, silt and clay.

The center and north-eastern parts of the catchment along with a narrow 300 m long band at the south-west of the catchment have a silty/sandy-silty surface horizon while the remaining half of the catchment is composed of a light sandy-silty layer.

With the exception of the outlet and several man-made and always dry segments, the entirety of the stream network lies in silty/sandy-silty surface horizon.

4 Discussion

4.1 Responses of discharge and groundwater level to precipitation events

Compared to the monthly average precipitation records from 1991-2020, compiled by Meteoswiss (*Normal values per measured parameter - MeteoSwiss* 2022 page), the monitoring period is relatively dry. According to these records, Chalet Villars meteostation (859 m a.s.l.), registers on average 101 mm of precipitation in April and 125 mm in May. When related to the monitoring period which lasted 32 days, with 9 in April and 23 in May, this gives an average precipitation of 123 mm for the monitoring period. However, total precipitations at Chalet Villars during the monitoring period was only 47.4 mm (Fig. 7), i.e. a precipitation deficit of 61.5%.

Hence, the following discussion derived from the analysis of precipitation data and dependant variables may only be representative of the middle of a dry spring season in the catchment of Bois-Vuacoz.

The discharge time series (Fig. 7) shows a clear reactivity to the occurring rainfall events. Each one of the five events results into a peak of the discharge measured at the outlet. Moreover, the shape of the discharge response of every event relates to the rainfall characteristics that triggered the discharge peak. As the discharge itself is related to the drainage density, it is interesting to start by investigating the influence of the rainfall characteristics on the discharge response. Events are compared to highlight how some rainfall characteristics shape the discharge response.

- The magnitude of the peaks appears to be positively correlated to the rainfall intensity. For example, the discharges measured at the start of events n°1 and 2 are respectively 32 and 47 L/min, both are closed to a tenth of the maximum discharge observed, 385 L/min. In addition, events n°1 and 2 have similar duration, respectively 6 and 4 h. However, these two events have very different average intensities, respectively 1.2 and 2.6 mm/h. As a result, the maximum discharges observed during these events are respectively 92 and 385 L/min, showing a 3-fold increase for event 1 and an 8-fold increase for event 2, compared to the discharge at the start of each event. Hence, the peak discharge during rainfall event seems to be strongly correlated to the intensity of the event.

- The duration of a precipitation event is positively correlated to the width of the discharge response as it can be seen when events n°2 and 3 are compared. Event n°2 presents a similar precipitation amount as event n°3 but is almost seven times shorter. While the magnitude of the discharge response of event n°2 is superior, the discharge remains above 200 L/min only 4 h for event n°2 compared to 14 h for event n°3.

- The fifth event presents a rounded shape in comparison to the others. It appears to be due to the long duration of the event, 10 h, combined with a small average intensity, 1.1 mm/h, and variation of this intensity throughout the event. This highlights the role of the variation of intensity as a rainfall characteristic of importance for the shape of the discharge response.

Description of the groundwater level time series (Fig. 7) showed that the groundwater level reacts to the catchment wetting triggered by precipitation events. However, the groundwater level response differs from the discharge one. In particular, two characteristics vary :

- Groundwater level peak is delayed of a few hours compared to the discharge peak. Events n°2 and 5 are clear examples, see the panels 3 and 4 of 8.

- In addition to delay, the shape of groundwater level and discharge peaks are also noticeably different. Taken as an example is the event n°5, the only event for which groundwater level time series contains the rising limb and the entire recession. The falling limb of the discharge shows a first phase characterised by a fast diminution of the discharge followed by a slower recession. If we take the discharge at the start of the peak as the reference level and the peak discharge as the maximum level, we observe that from the moment the discharge starts to rise, it takes 18 h to fall back to 50% of the maximum and 78 h to get back to the reference level. In comparison, the groundwater level falling limb indicates a slower recession. Indeed, if we take as the reference level the groundwater level measured at the start of the peak and as the maximum level the highest value of the peak, we observe that from the moment the groundwater level starts to rise, it takes 89 h to fall back to 50% of the maximum and 133 h to get back to the reference level.

Discharge response to a rainfall event is mostly constituted by superficial flow. Figure 22 shows that soils below the stream network have a sandy texture. Sandy soils are characterised by their good infiltration rate. They can indicate the presence of fast subsurface flow paths toward the stream channels. An hypothesis further supported by the small surface area of the catchment and the density of the stream network. The combination of both can trigger a sharp discharge peak. The third and fourth panels of Figure 8 illustrate the fast response experienced by the discharge in reaction to the precipitation event compared to the delayed groundwater level response. Groundwater level delay certainly comes from the time needed by the infiltrated water to reach the water table. Infiltration rate can reasonably assumed to be slower than the velocity of water in superficial flow paths. Once the water begins to reach the water table, its level starts to increase. It is also probable that as the water table rises, groundwater start to feed the streams, causing the second step of the discharge rising limb, see in Fig. 8. In this particular catchment, the expansion is more likely to be bottom-up. The shallow depth of the soil in the lower-lands at the north-west of the catchment, illustrated in Fig. 21, combined with a clayey bedrock formation favor the presence of a water table close to the surface, more likely to lose water to the streams in case of precipitation.

For the same reason, discharge and and groundwater level experience delayed peak values.

As for the recession phase, the groundwater level starts to recess when the water inputs can not match the export of water toward the stream channels and the lower hill-slope. However, this process is controlled by the relatively slow velocity of the groundwater. The retention of the water by the ground causes the recession phase to be longer than the discharge one. And indeed, the description of the recession phases

of groundwater level and discharge for event n°5 is consistent with my assumption.

4.2 Analysis of the computed drainage density

The shape of the modelled drainage density time series is squared. Abrupt variations in the time series are caused by the discontinuous and finite number of values taken by the drainage density as a result of the method used to compute it. In particular the allocation of multiple stream reaches to sensor locations is later resulting in sudden activation and deactivation of large parts of the network at the exact same time. For instance, as detailed in Fig. 2, the sensor location B5 has 555.6 m of stream allocated to it, which represents 17.3% of the whole network, the most of all the sensor locations. B5 happens to have an hydrological behavior really suited to describe the behavior of an important number of stream reaches, as observed in the four mapping surveys. While these segments have certainly the same hydrological state evolution across wet and dry periods, this particular way of connecting their behavior to a sensor location does not take into account the subtle variations of activation and deactivation times between these reaches.

Concerning the small number of values taken by the drainage density it is also linked to the limited percentage of sensor locations with a persistence which is neither 0% or 100%. As detailed in the Table 5, 60% of the stream network length remained in the same during the entire monitoring period. On the 17 sensor locations, 10 of them flowed continuously, including the 5 water-level sensor locations, and two never experienced flow. Therefore, only 5 sensor locations substantially contributed to the variations of the drainage density. This severely limited the number of values taken by the modelled drainage density. In order to obtain better data, I could have installed more sensors at critical locations. This would allow to have accurate stream state information for more streams and would reduce the number of segments allocated to each sensor location. Combined with more mapping surveys to improve the segment allocation, the computed drainage density would be more accurate and would provide more detailed variations.

For both wet periods, the drainage density varied from a starting value of 4.64 km/km^2 and reached an upper-limit at a computed value of 9.07 km/km^2. This represents a maximum drainage density change of 4.43 km/km^2 during the rainfall events. The stream network expands twice its starting length. For the first wet period, this change starts during the event n°1 and end at the beginning of event n°2. During the second wet period, only the event n°5 is necessary to record this variation.

For each wet period, the drainage density plateaued several hours before discharge and groundwater level peaks. In addition, the upper-limit of drainage density appears to be common for two very different wet periods, both in terms of duration (resp.76 h and 10 h) and total precipitation (resp.32.2 mm and 11 mm). These elements tend to place the value of 9.07 km/km^2 as the uppermost value reachable to the stream network. A limit to which the drainage density is physically constrained by the extent of the geomorphological channel network. The theoretical maximum drainage density, calculated from the

stream network mapping, is 12.84 km/km^2. Ca. one fourth of the network length never flowed according to the computed drainage density. A large proportion of the stream reaches with a flowing persistency of 0% consist in man-made channels seemingly not favourable to host stream flow.

As the monitoring period is relatively short and dry, the assumption of a drainage density constrained to 9.07 km/km^2 could no longer hold if a monitoring of the stream network was realised during wetter periods, like successive intense rainfall events.

Figure 8 shows that the onset of drainage density is correlated to the groundwater level as both of them start to increase simultaneously.

The calculation method of the drainage density does not translate the real slight variations leading to the peak drainage density. Instead, for each sensor detecting flow, several allocated reaches are considered activated. Therefore, the timing of the upper-limit observed by the drainage density remains difficult to estimate with precision. However, it seems that the end of the drainage density rising limb is more correlated to the discharge than the groundwater level. As for the length of the drainage density peak, it seems correlated to the discharge level.

While the expansion of the stream network at the beginning of both wet periods happens in a similar timespan, the contraction reveals two different time scales. First, the drainage density remains at the upper-limit 1.5 times longer for the first wet period after the end of the last precipitation recorded. Secondly, the contraction process between the plateau value and the base value lasts more than 3 times longer for the first wet period. I support the hypothesis that the timespan of the drainage density recession phase is driven by the wetness of the catchment brought by the amount of precipitation fallen during the event or succession of events. Indeed, the first wet period has seen an amount of precipitation 3 times superior to the second wet period.

After both wet periods, at the end of the stream network contraction phase, a base value of 3.92 km/km^2 is reached. For a prolonged period of time, between the 08th and the 19th of May, the drainage density stays constant despite negligible precipitation amounts. This behavior deviate from the steady decrease of the discharge and groundwater level during the same time interval. Nevertheless, as the modelling allocate whole segments to point measurements, it may hide a slow drainage density decrease as the catchment dries up. In particular, in the less shady parts of stream reaches or at flatter locations, the transition from flowing to standing water or even dry stream bed might occur sooner than at sensor locations. Furthermore, the drainage density is obtained from the flowing state which does not take into account the discharge evolution as long as it exceeds a certain threshold.

From the 19th of May, the constant drainage density starts to decrease. During daytime, the flow sensor at location B9 registers a cessation of the flow. At the same period the flow sensors of B11, B12

and B15 have been incapable of recording the very weak values of the flow (<0.5 L/min) during the time. In these cases, a manual correction of the flow state has been realised as a field survey could confirm a sensor malfunction. However, in B9 case, no malfunction of the flow sensor could be detected and as a consequence no correction of the flow state has been performed. Nevertheless, I hypothesize that the observed diurnal pattern is a consequence of the variations in the groundwater level. As the water table decreases and is subject to diurnal pattern, some activated streams reach a point were they are not fed by groundwater flow during daytime.

4.3 Relationship between drainage density and catchment discharge

(Godsey and Kirchner 2014) observed that the drainage density varied as a power function of discharge in the networks they studied and in networks coming from published surveys. We tested this assumption by fitting a power-law between the drainage density and the discharge, see Fig. 9. The model is not satisfactory. Visually, it does not explain the behavior of drainage density for low and high values.

The β exponent of the fitted power-law has a value of 0.20, in the very low range of the interval [0.18,0.40] proposed by Godsey and Kirchner (2014) from their summarizing work on published surveys.

At the BV catchment, low drainage density values are associated to a larger range of discharge than higher drainage density values. The data points concerned have been collected during dry periods, in between events. During these intervals of time, while the discharge receded, a constant number of stream reaches continued to flow. It could be that the lowest drainage density value corresponds to the minimum extent of the stream network during dry period at this time of the year. Activated stream reaches during theses periods are in the down-hill section of the catchment. They are fed by longer-term water storage than higher-up streams in the catchment. This may indicates that the groundwater level is situated further to the surface in higher-up areas compared to the valley where the main stream flows. In addition, the action of gravity might favor groundwater flow from higher-up areas toward the valley and create a situation where the groundwater table in the valley is replenished by the water infiltrated in higher-up areas.

The color code in Fig. 9 highlights the existence of two clusters of points. On the lower-left and in the center of the figure, we can find all the points belonging to periods characterised as dry. The top-right corner of the figure contains all the points captured during rainfall periods. These two clusters visually demonstrate that different relationships exist between the drainage density and the discharge when the catchment undergoes a rainfall event and when it is not.

The subset of data points captured during rainfall events can be further divided in two categories : points where drainage density is correlated to discharge and points where the drainage density has reached its maximum boundary and does not react to any further increase in discharge. The Fig. 10 assembles the three described phases and propose a model adapted to each one of them. The necessity to use a more

complex model compared to precedent studies certainly comes from the 10 minutes temporal resolution which is sufficiently fine to reveal the different behaviors undergone by the drainage density depending on the discharge. As we have seen that the discharge is sensitive to the catchment wetness conditions, the drainage density also appears to vary accordingly. Below a certain catchment wetness, around 15 L/min on Fig. 10, the drainage density stops varying and keeps a constant base value. Above a certain catchment wetness, approximately 150 L/min on Fig. 10, the drainage density can no longer increase and remains at a constant maximum value. In between these two catchment wetness conditions, the drainage density is correlated to the the catchment wetness.

The power-law model used explains the general variation of the drainage density as a function of the discharge. However, the coefficient of determination with a value of 0.50 quantifies the important proportion of data scattering around the curve which is not explained by the model. A detailed observation of the relationship between drainage density and discharge during rainfall events reveals the presence of an hysteresis loop.

The Figure 19 focuses on the relationship between drainage density and discharge during the rainfall event n°5. We can observe a counter-clockwise hysteresis loop between drainage density and discharge. The stream network expansion, expressed as an increase of the drainage density, and the discharge have similar timings when it comes to the rising phase. However, the hysteretic pattern emerges as the contraction of the network starts approximately a day after the discharge recession begins.

At first, drainage density and discharge are rising driven by superficial flows occurring as the rainfall event is still going on. The drainage density appears to reach its upper limit in first and starts to stagnate while the discharge continues to increase as it is not constrained by the size of the channel it flows in. As the event finishes, the discharge initiates a recession. At the same time the drainage density continues to plateau. As it is constrained by the extent of its geomorphological channel network, it does not need as much water input as the discharge to maintain its upper-limit. As the flow paths feeding the discharge and the drainage density continue to fade, the drainage density ultimately begins to decrease as well. The presence of a hysteresis loop proves that the expansion and contraction of the drainage density can not be accurately described by the same modelled function. The next modelling step could be to divide into two the subset of data used to model the power-law. One subdivision would contain the data points recorded during expansion of the drainage density and the other would encompass the data points captured during the contraction of the drainage density. For each of them, a different model could be tested.

4.4 Relationship between drainage density and groundwater level

No scientific article published in review has tested the relationship between the drainage density and the groundwater level. In a semester project for the ECHO lab (Buchs 2021), Guillaume Buchs analysed the data from Langried, a montane headwater catchment located in Switzerland. He fitted a power-law and and linear regression between the drainage density and the groundwater level. He concluded that

while the linear fitting seemed more suited than the power-law, both model could not accurately represent the behavior of the drainage density when it reaches its upper-limit.

In order to test the existence of a relationship, I fitted a power-law and a linear regression to the drainage density and the groundwater level, see Fig. 11 and 12. Both plots are visually similar to Fig. 9 representing the fitted power-law between drainage density and discharge. In both plots, we observe the same features, i.e. a subset of data points at the lowest drainage density value for which the groundwater level takes a large range of value, a similar subset at the upper-limit of drainage density and a mid-range zone where the drainage density and the groundwater level are positively correlated. Both models are not able to accurately represent these different relations between the variables.

The Figure 13 models the relationship between drainage density and groundwater level in three segments. This modelling does not work as well as for the relationship between drainage density and discharge (see Fig. 10). Unlike with the discharge, the three subset of points corresponding to the three phases of the relationship are largely overlapping. As a result, the connections between the three segments of the model does not reproduce the real variations of the data. The temporal groundwater variations are slower and smoother compared to the discharge. In addition, the variations present a delay to those occurring to the drainage density. This combination of factors creates an overlapping between the three observed phases of the relationship between drainage density and groundwater level. Modelling effectively this relationship seems to present more difficulty than modelling the relationship between drainage density and discharge. Concerning the segment modelled with a power-law function, while the coefficient of determination is higher than the one derived for the power-law between drainage density and discharge (Fig. 10), the scattering around the data is also present. Its presence is due to a hysteresis loop.

The Figure 20 focuses on the relationship between drainage density and groundwater level during the rainfall event n°5. We observe a clockwise hysteresis loop between drainage density and groundwater level, the opposite rotation direction to the one involving drainage density and discharge.

The recession of the water table appears to be a slower process than the contraction of the stream network. In the ground, the water velocity is controlled by the permeability of the layers it travels trough. While the presence of sand in the soil and in the geotype layer favor a good permeability, the water velocity in the streams and in subsurface flow paths remains superior. Moreover, the flatness of the catchment might results in low hydraulic gradients in the aquifer and ultimately in a relatively slow groundwater velocity. The hysteresis loop creates some scattering around the power-law model. Expansion and contraction of the drainage density could use two separate models.

4.5 Stream network expansion in relation with antecedent wetness and rainfall properties

The Figure 18 details the drainage density variations from the start of the rainfall event n°1 to the end of the recession of event n°4. In addition, antecedent wetness calculated as the sum of precipitation fallen in the 72 h before the start of each event is added to the individual figures describing the events (Fig. 14, 15, 16 and 17).

The first event has a null antecedent wetness. The drainage density occurring during this event is relatively low, only one third of the maximum possible variation if the maximum drainage density was reached. A null antecedent wetness can potentially indicate a dry unsaturated zone with an important storage capacity and an important infiltration rate. As the precipitation from the first event falls, the rain will preferentially recharge the unsaturated zone without setting in motion numerous flow paths feeding the stream network. The resulting network expansion is limited.

A few hours after the first event comes event n°2. The antecedent wetness is greater than zero. The occurring drainage density positive change is twice as important as the first event. As shown by the antecedent wetness, the catchment wetness has increased. The unsaturated zone is already starting to recharge and the infiltration rate may even have decreased. As a result, the event n°2 prompts a greater stream network expansion than event n°1.

Events n°3 and 4 start with an antecedent wetness several times greater than event n°2. However, no drainage density change occurs during each one of them. This demonstrate that over a certain catchment antecedent wetness, the drainage density reaches its maximum boundary and the stream network can not expand anymore to respond to further wetting of the catchment.

With the set of data used for the analysis, it is not possible to disentangle for each event the proportion of change in drainage density caused by antecedent wetness from the one produced by the amount of precipitation. The combination of both a larger antecedent wetness and precipitation amount is the cause of the greater drainage density increase happening during event n°2 in comparison to event n°1. Nevertheless the precipitation amount appears to be positively correlated to the positive change in drainage density during a rainfall event.

4.6 Stream network extent and soils properties

Figures 21 and 22 reveal that the stream network mostly extends on soils with particular properties. A vast majority of the stream reaches and importantly most of the reaches with a persistency greater than zero are found on a soil that combine a depth lower than 50 cm and a lower proportion of sand in its composition compared to the remaining areas of the catchment. Below the soil layers, the first geological layer and the bedrock underneath contain clay, a material known for its low permeability. This configuration hints toward the presence of a superficial groundwater table in the low-lands of the

catchment, where the main stream and the principal tributaries flow.

In the south-west and north-east parts of the catchment, a sandier and deeper soil might favors the infiltration of rainfall. The infiltrated water might recharge the ground aquifer or gain the stream via subsurface flow paths. By ensuring a replenishment of the groundwater, this area contributes to the flow permanence of the main stream during dry periods of time.

4.7 Diurnal patterns in discharge and groundwater level

After the end of the fifth event, both the discharge and groundwater experience diurnal patterns, noticeable on third and fourth panels of 7. During dry periods, shallow flow paths are progressively deactivated and the discharge principally depends on the base flow. Base flow is fed by groundwater storage and delayed subsurface storage (Price 2011). In these conditions, catchment discharge can present a higher correlation to groundwater level than during rainfall event.

According to Gribovszki (Gribovszki, Szilágyi, and Kalicz 2010), diurnal fluctuations of stream flow and groundwater level in forested catchments finds its origin in evapotranspiration induced by riparian vegetation in spring and summer. During day, plants try to meet their water demand from the groundwater, causing the water table to lower. During night, the replenishment of the groundwater is partially possible as the evapotranspiration term becomes smaller. However, for the groundwater level measured at Bois-Vuacoz, the replenishment at night is not sufficient to prevent the water table to progressively fall, as it can observed from the 12th to the 23rd of May in the last panel of 7. It indicates that the replenishment term can not compensate a series of high evapotranspiration days. In fact, groundwater replenishment is proven to be more efficient where an important hydraulic gradient exist favoring the uptake of water in depleted zones. The groundwater well in BV catchment is situated in the flat upper-lands of the catchment and close to the main stream, see on Fig. 6. Therefore, it may exfiltrate more water toward the main stream than it can receive from higher sections of hill-slope.

4.8 Limitations

Some limitations have impacted the analysis. The loss of data from several sensors imposed us to shorten the monitoring period initially planed. Consequently, our results might be representative to the specific conditions we captured, that is to say a relatively dry year and month, in spring and a few weeks after the snow melt. Thus, our findings might not hold during different conditions.

5 Conclusion

In the Bois-Vuacoz catchment, the largest computed drainage density increase during a rainfall event was from 4.64 km/km^2 to 9.07 km/km^2. The flowing stream network doubled in length. 9.07 km/km^2 was the observed maximum boundary of drainage density. It was the maximum extent of the stream network, the value from which the drainage density did not react to further catchment wetting. Never activated mapped channels revealed to be man made and did not contribute to the expansion of the stream network during rainfall events. Between rainfall event, when the catchment dried up, I observed a minimum boundary to the drainage density, between 3.33-3.92 km/km^2. A fixed number of stream reaches, most belonging to the main stream and situated in the catchment valley area, demonstrated flow permanency. I hypothesized that the groundwater table feeding these streams was replenished by the infiltration of water in the sandy and relatively deep soils characterising the higher areas of the catchment.

To reproduce the respective relationships of drainage density with discharge and with groundwater level, I used a model composed of three segments. Two constant functions represented the minimum and maximum boundaries of drainage density. In between, the middle segment was a power-law function to model the positive correlation of drainage density with discharge, resp. groundwater level, in between the boundaries. In the case of discharge, this approach correctly represented the successive phases of the relationship with drainage density but for groundwater level, the model was not suited as the three phases of the relationship with drainage density overlapped in the same range of groundwater levels. In both cases, the existence of an hysteresis loop between drainage density and discharge, resp. groundwater level, during the expansion and contraction of the stream network during a rainfall event, created scattering of the data around the modelled power-law. Distinct modelling of expansion and contraction phases could improve the accuracy of the model.

During rainfall events, an increase in antecedent wetness resulted in larger positive variation of the drainage density, until the drainage density reached its maximum boundary. At this limit, the drainage density did no longer increase and stopped responding to antecedent wetness positive variation. The precipitation amount fallen during a rainfall event was positively correlated with the increase in drainage density. However, the analysis did not allow to disentangle the respective contribution of antecedent wetness and precipitation amount on drainage density variation during a rainfall event.

Appendices

A Outlet discharge rating curve

Bois-Vuacoz outlet discharge rating curve with discharge Q in [L/min] and water-level WL in [cm] :

$$Q = 1.49880 * WL^{2.29626} \tag{4}$$

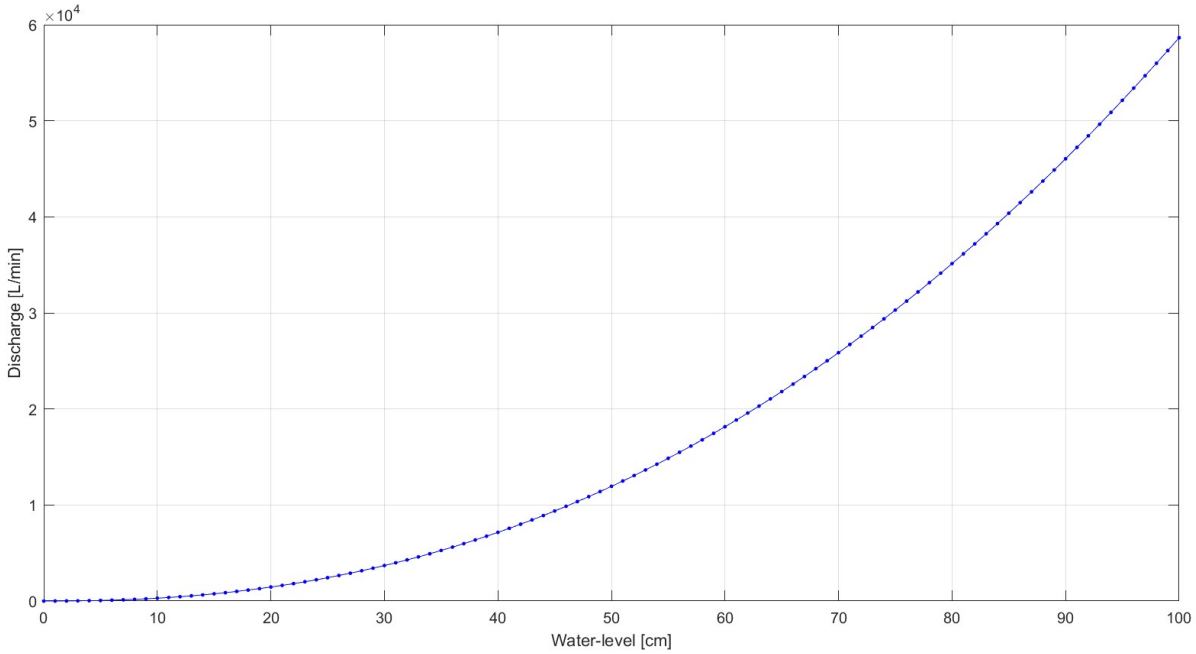

Figure A.1: Bois-Vuacoz outlet discharge rating curve

B Stream reach allocation

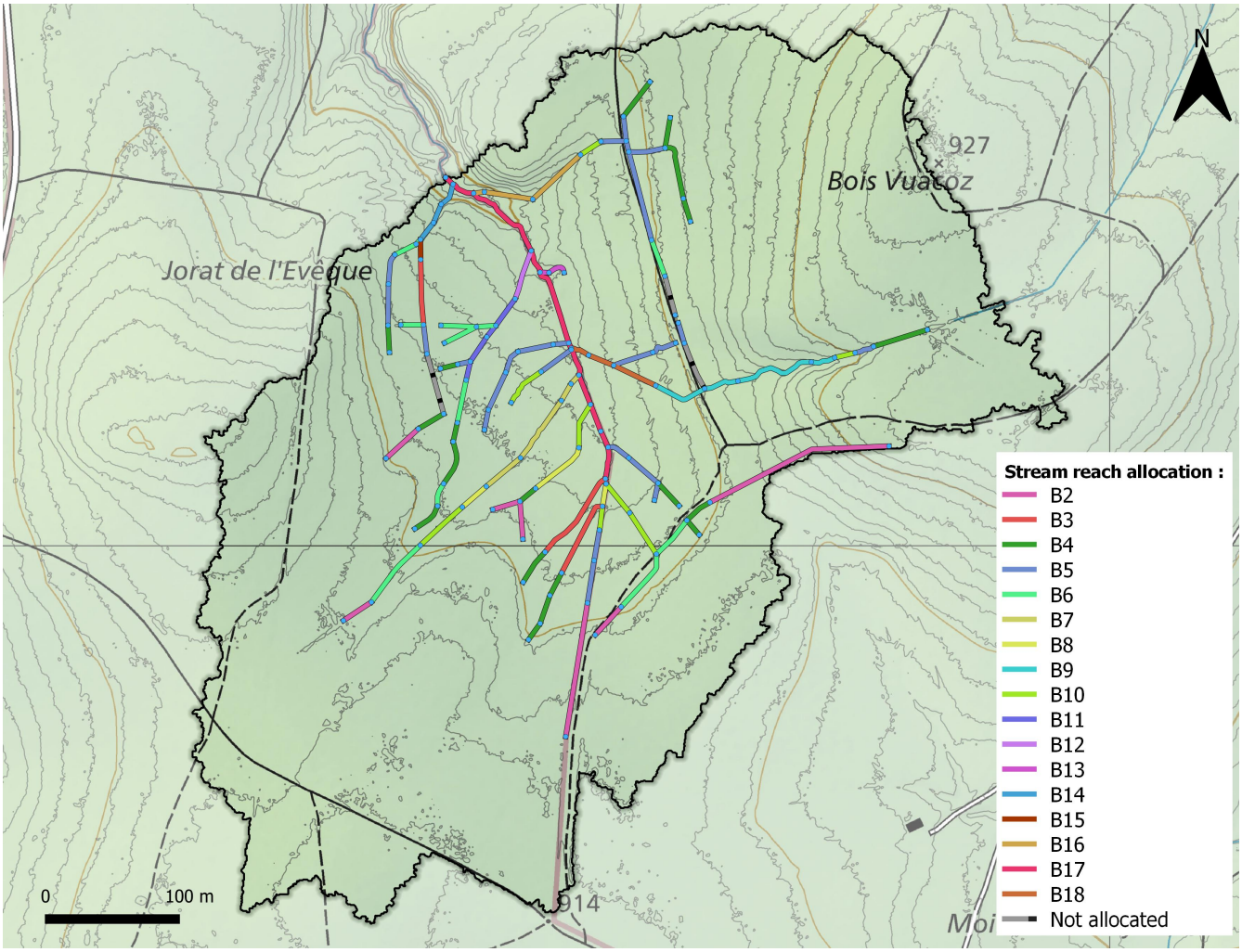

Figure B.1: Stream reach allocation to sensor location

References

Acuña, V. et al. (Mar. 7, 2014). "Why Should We Care About Temporary Waterways?" In: *Science* 343.6175. Publisher: American Association for the Advancement of Science, pp. 1080–1081. DOI: 10.1126/science.1246666. URL: https://www.science.org/doi/10.1126/science.1246666 (visited on 07/16/2022).

Angeles, Raphaël (2022). *Mapping temporary streams in the Haute Mentue catchment*. Semester project. Ecole Polytechnique Fédérale de Lausanne. (Visited on 07/16/2022).

Assendelft, Rick S. and H. J. Ilja van Meerveld (Jan. 2019). "A Low-Cost, Multi-Sensor System to Monitor Temporary Stream Dynamics in Mountainous Headwater Catchments". In: *Sensors* 19.21. Number: 21 Publisher: Multidisciplinary Digital Publishing Institute, p. 4645. ISSN: 1424-8220. DOI: 10.3390/s19214645. URL: https://www.mdpi.com/1424-8220/19/21/4645 (visited on 07/16/2022).

Buchs, Guillaume (2021). *Predicting stream network expansion and contraction*. Semester project. Ecole Polytechnique Fédérale de Lausanne. (Visited on 07/20/2022).

Creed, Irena F. et al. (Nov. 2017). "Enhancing protection for vulnerable waters". In: *Nature Geoscience* 10.11. Number: 11 Publisher: Nature Publishing Group, pp. 809–815. ISSN: 1752-0908. DOI: 10.1038/ngeo3041. URL: https://www.nature.com/articles/ngeo3041 (visited on 07/19/2022).

Day, D. G. (1978). "Drainage density changes during rainfall". In: *Earth Surface Processes* 3.3, pp. 319–326. ISSN: 1931-8065. DOI: 10.1002/esp.3290030310. URL: https://onlinelibrary.wiley.com/doi/abs/10.1002/esp.3290030310 (visited on 07/16/2022).

Godsey, S. E. and J. W. Kirchner (2014). "Dynamic, discontinuous stream networks: hydrologically driven variations in active drainage density, flowing channels and stream order". In: *Hydrological Processes* 28.23, pp. 5791–5803. ISSN: 1099-1085. DOI: 10.1002/hyp.10310. URL: https://onlinelibrary.wiley.com/doi/abs/10.1002/hyp.10310 (visited on 07/16/2022).

Goulsbra, Claire, Martin Evans, and John Lindsay (2014). "Temporary streams in a peatland catchment: pattern, timing, and controls on stream network expansion and contraction". In: *Earth Surface Processes and Landforms* 39.6, pp. 790–803. ISSN: 1096-9837. DOI: 10.1002/esp.3533. URL: https://onlinelibrary.wiley.com/doi/abs/10.1002/esp.3533 (visited on 07/16/2022).

Gribovszki, Zoltán, József Szilágyi, and Péter Kalicz (May 7, 2010). "Diurnal fluctuations in shallow groundwater levels and streamflow rates and their interpretation – A review". In: *Journal of Hydrology* 385.1, pp. 371–383. ISSN: 0022-1694. DOI: 10.1016/j.jhydrol.2010.02.001. URL: https://www.sciencedirect.com/science/article/pii/S0022169410000685 (visited on 07/17/2022).

Guichet cartographique du canton de Vaud (2022). URL: https://www.geo.vd.ch/ (visited on 07/16/2022).

Haute-Mentue catchment (2005). URL: https://echo2.epfl.ch/mentue/pages/Mentue_accueil_instruments.htm.

janavonfreyberg.com (2022). URL: https://www.JanaVonFreyberg.com/temporary-streams-tempaqua.html (visited on 07/18/2022).

Joerin, Christophe (2000). "Etude des processus hydrologiques par l'application du traçage environnemental: association à des mesures effectuées à l'échelle locale et analyse d'incertitude". Thèse de doctorat. Lausanne: EPFL (Ecole Polytechnique fédérale de Lausanne). 234 p. URL: https://doc.rero.ch/record/4705 (visited on 07/16/2022).

Meerveld, H. J. I. van et al. (2019). "Expansion and contraction of the flowing stream network alter hillslope flowpath lengths and the shape of the travel time distribution". In: *Hydrology and Earth System Sciences* 23.11, pp. 4825–4834. DOI: 10.5194/hess-23-4825-2019. URL: https://hess.copernicus.org/articles/23/4825/2019/.

Meyer, Judy L. et al. (2007). "The Contribution of Headwater Streams to Biodiversity in River Networks1". In: *JAWRA Journal of the American Water Resources Association* 43.1, pp. 86–103. ISSN: 1752-1688. DOI: 10.1111/j.1752-1688.2007.00008.x. URL: https://onlinelibrary.wiley.com/doi/abs/10.1111/j.1752-1688.2007.00008.x (visited on 07/16/2022).

Nadeau, Tracie-Lynn and Mark Cable Rains (2007). "Hydrological Connectivity Between Headwater Streams and Downstream Waters: How Science Can Inform Policy1". In: *JAWRA Journal of the American Water Resources Association* 43.1, pp. 118–133. ISSN: 1752-1688. DOI: 10.1111/j.1752-1688.2007.00010.x. URL: https://onlinelibrary.wiley.com/doi/abs/10.1111/j.1752-1688.2007.00010.x (visited on 07/16/2022).

Normal values per measured parameter - MeteoSwiss (2022). Meteoswiss. URL: https://www.meteoswiss.admin.ch/home/climate/swiss-climate-in-detail/climate-normals/normal-values-per-measured-parameter.html (visited on 07/16/2022).

Peirce, Sarah E. and John B. Lindsay (2015). "Characterizing ephemeral streams in a southern Ontario watershed using electrical resistance sensors". In: *Hydrological Processes* 29.1, pp. 103–111. ISSN: 1099-1085. DOI: 10.1002/hyp.10136. URL: https://onlinelibrary.wiley.com/doi/abs/10.1002/hyp.10136 (visited on 07/16/2022).

Price, Katie (Aug. 1, 2011). "Effects of watershed topography, soils, land use, and climate on baseflow hydrology in humid regions: A review". In: *Progress in Physical Geography: Earth and Environment* 35.4.

Publisher: SAGE Publications Ltd, pp. 465–492. ISSN: 0309-1333. DOI: 10.1177/0309133311402714. URL: https://doi.org/10.1177/0309133311402714 (visited on 07/17/2022).

Rinaldo, Andrea, Marino Gatto, and Ignacio Rodriguez-Iturbe (Feb. 1, 2018). "River networks as ecological corridors: A coherent ecohydrological perspective". In: *Advances in Water Resources* 112, pp. 27–58. ISSN: 0309-1708. DOI: 10.1016/j.advwatres.2017.10.005. URL: https://www.sciencedirect.com/science/article/pii/S0309170817305717 (visited on 07/16/2022).

Schiller, Daniel von et al. (Jan. 1, 2017). "Chapter 3.2 - Nutrient and Organic Matter Dynamics in Intermittent Rivers and Ephemeral Streams". In: *Intermittent Rivers and Ephemeral Streams*. Ed. by Thibault Datry, Núria Bonada, and Andrew Boulton. Academic Press, pp. 135–160. ISBN: 978-0-12-803835-2. DOI: 10.1016/B978-0-12-803835-2.00006-1. URL: https://www.sciencedirect.com/science/article/pii/B9780128038352000061 (visited on 07/16/2022).

Stubbington, Rachel et al. (2017). "Temporary streams in temperate zones: recognizing, monitoring and restoring transitional aquatic-terrestrial ecosystems". In: *WIREs Water* 4.4, e1223. ISSN: 2049-1948. DOI: 10.1002/wat2.1223. URL: https://onlinelibrary.wiley.com/doi/abs/10.1002/wat2.1223 (visited on 07/16/2022).

Acknowledgments

I would like to express my gratitude to Dr von Freyberg for her sound guidance and useful critiques from which I greatly benefited. I would also like to thanks Ms Bujak for her constructive suggestions and willingness to help me throughout this research work. To both of them, I wish to express that their enthusiasm for the study of temporary streams was inspiring and motivating.

To Mr Karapancsev, Mr Luder, Mr Léveillé and Mr Angeles, I wish to adress my recognition for the quality of their collaboration during field work. For the unwavering support they provide me, I would like to thanks my family and my friends.